

**This is the accepted manuscript version of the contribution published as:**

Espinoza Miranda, S.S., **Abbaszade, G.**, Hess, W.R., Drescher, K., Saliba, A.-E., Ziburdaev, V., Chai, L., Dreisewerd, K., Grüneberger, A., Westendorf, C., **Müller, S.**, Mascher, T. (2025):

Resolving spatiotemporal dynamics in bacterial multicellular populations: approaches and challenges

*Microbiol. Mol. Biol. Rev.* 89 (1), e00138-24

**The publisher's version is available at:**

<https://doi.org/10.1128/mnbr.00138-24>



50	<b>Table of contents</b>	
51		
52	Introduction	3
53	1. Analysis of spatiotemporal distribution of single cells in intact biofilms by microscopy	8
54	2. Analysis of the spatial distribution of metabolites and structural lipids in bacterial colonies	
55	and biofilms using mass spectrometry imaging	10
56	3. Analysis of single-cell heterogeneity and its local dynamics by microbial flow cytometry	13
57	4. Analysis of early biofilm development and behavior by microfluidic cultivation systems	16
58	5. Analysis of cellular function in single cells: Single-cell transcriptomics	19
59	5.1. Challenges associated with capturing the RNA of a single bacterium	20
60	5.2. Single-bacteria RNA-seq using combinatorial methods	21
61	5.3. Single-bacteria RNA-seq on plates	22
62	5.4. Single-bacteria RNA-seq in droplets	22
63	5.5. Spatial transcriptomics for bacteria	22
64	6. Analysis of biophysical properties of intact biofilm populations	25
65	6.1 Fluorescence microscopy-based microrheology	26
66	6.2 Optical elastography	26
67	6.3 X-ray synchrotron diffraction and fluorescence	28
68	Conclusions	29
69	Acknowledgements	30
70		
71		
72		
73		
74		
75		
76		
77		
78		
79		
80		
81		
82		
83		
84		
85		
86		
87		

88 **Abstract**

89 The development of multicellularity represents a key evolutionary transition that is crucial  
90 for the emergence of complex life forms. Although multicellularity has traditionally been  
91 studied in eukaryotes, it originates in prokaryotes. Coordinated aggregation of individual  
92 cells within the confines of a colony results in emerging, higher-level functions that benefit  
93 the population as a whole. During colony differentiation, an almost infinite number of  
94 ecological and physiological population-forming forces are at work, creating complex,  
95 intricate colony structures with divergent functions. Understanding the assembly and  
96 dynamics of such populations requires resolving individual cells or cell groups within such  
97 macroscopic structures. Addressing how each individual cell contributes to the collective  
98 action requires pushing the resolution boundaries of key technologies that will be  
99 presented in this review. In particular, single-cell techniques provide powerful tools for  
100 studying bacterial multicellularity with unprecedented spatial and temporal resolution.  
101 These advancements include novel microscopic techniques, mass spectrometry imaging,  
102 flow cytometry, spatial transcriptomics, single-bacteria RNA-seq, and the integration of  
103 spatiotemporal transcriptomics with microscopy, alongside advanced microfluidic  
104 cultivation systems. This review encourages to explore the synergistic potential of the  
105 new technologies in the study of bacterial multicellularity, with a particular focus on  
106 individuals in differentiated bacterial biofilms (colonies). It highlights how resolving  
107 population structures at the single-cell level and understanding their respective functions  
108 can elucidate overarching functions of bacterial multicellular populations.

109  
110 **Keywords:** microbial multicellularity, population ecology, phenotypic heterogeneity, cell  
111 differentiation, single-cell technologies, single-cell transcriptomics, population dynamics  
112

113  
114 **Introduction**  
115

116 The development of multicellularity represents a pivotal evolutionary transition, laying the  
117 foundation for the emergence of complex life forms on Earth (1). Unlike many evolutionary  
118 events, multicellularity has risen independently and multiple times, particularly in the  
119 bacterial kingdom (2–4). While the emergence of complex multicellularity in prokaryotes  
120 dates back some three billion years, the current knowledge of this process is still  
121 predominantly derived from studies of eukaryotic organisms (5). The general concept of  
122 multicellularity encompasses several critical developmental requirements including cell  
123 adhesion, cell-cell communication, cell-cell coordination, functional diversification and  
124 interactions among cells, defense mechanisms or programmed cell death.

125

126 Ever since Robert Koch's postulates, which required isolating pure cultures of  
127 microorganisms from individual cells, bacteria were – and still are – perceived as  
128 archetypically unicellular. While multicellular traits are well documented for some species,  
129 most prominently the filamentous cyanobacteria, streptomyces, or myxobacteria, these  
130 examples were appreciated as fascinating multicellular exceptions from an otherwise  
131 unicellular bacterial world (6–9). However, an appreciation of 'common' bacteria as  
132 multicellular organisms started only very slowly, with two seminal conceptual articles by  
133 James Shapiro (10, 11). Since then, the diversity and inherent phenotypic heterogeneity  
134 of bacterial populations has been recognized by an increasing number of studies. What  
135 once seemed homogeneous – as the average of a population – suddenly became  
136 visible as highly heterogeneous. Isogenic populations diversify into phenotypically  
137 different subpopulations and cell types that are endowed with astonishing individuality  
138 (12, 13).

139  
140 Developing a concept for bacterial multicellularity is still at its beginning, but the  
141 underlying field of research is currently fast evolving, as also highlighted by this review.  
142 Accordingly, no generally accepted definition exists and any attempt remains an  
143 approximation towards a universally acceptable concept to come. For many, bacterial  
144 multicellularity is only applicable (if at all) to terminally differentiated cell states within  
145 larger population aggregates, such as fruiting bodies, (endo)spores or heterocysts. While  
146 such a definition is in line with the eukaryotic concept of multicellularity, in which cells  
147 terminally differentiate to assume their functions in the context of tissues and organs (14),  
148 it neglects the important role of non-terminally differentiated cells in the context of  
149 bacterial biofilms. While it can be argued that phenotypically diversified cells in biofilms  
150 and structured colonies only follow, and then adapt to, local gradients and accordingly  
151 should not be considered as multicellular states, this restricted perception neglects the  
152 truly multicellular driving forces behind the evolution of such traits.

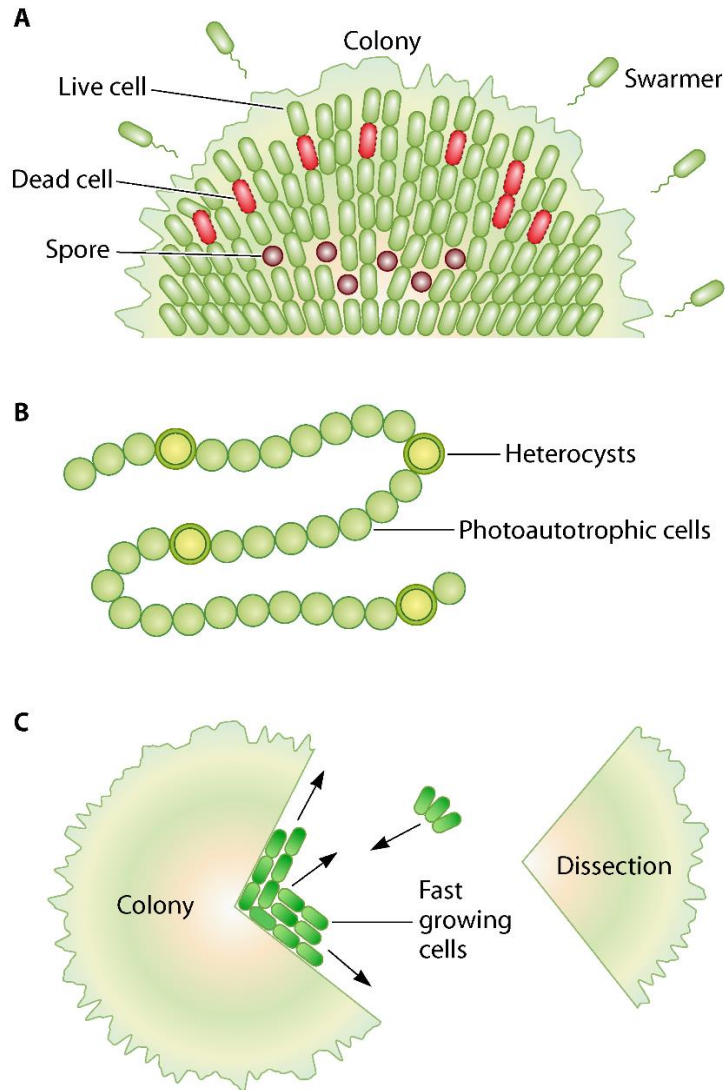
153  
154 For the purpose of this review, we propose a more comprehensive definition of bacterial  
155 multicellularity as characterized by spatially structured bacterial populations that exhibit  
156 at least transient stability. Multicellularity encompasses several key elements: (i) cellular  
157 differentiation (15) and the dynamic distribution of different cell types (**Figure 1A**), (ii)  
158 positional determinants that govern cell positioning and influence cell fate (**Figure 1B**),  
159 (iii) a distinct architectural organization of the microbial population governed by (iv)  
160 extracellular cues and biophysical properties, including chemical gradients (nutrients,  
161 oxygen, antibiotics), which determine and are shaped by (v) intercellular interactions and  
162 the interplay between cells and their environment (**Figure 1C**). Collectively, these aspects  
163 determine the form of bacterial multicellularity (filament, biofilm, differentiated colony) that  
164 provides a structural framework, from which emergent multicellular functions can arise.

165

166 'Form' and 'Function' are therefore tightly interconnected aspects of bacterial  
167 multicellularity that critically depend on each other. True multicellular functions can only  
168 emerge in the context of a differentiated multicellular form. The multicellular form  
169 presumably evolved only, because it provided an overall fitness advantage to the entire  
170 population that outweighed any costs associated with a multicellular lifestyle. Importantly  
171 for this concept of multicellularity, such functions either exclusively occur in a multicellular  
172 form or at least only make physiological sense within its context. These functions provide  
173 a fitness gain for the population. Accordingly, the differentiated multicellular population  
174 rather than the individual cell is the unit of evolution for such traits to manifest, irrespective  
175 of whether the underlying physiology leads to a terminally or only transiently differentiated  
176 cell within a stable multicellular population.

177  
178 The ability to process large amounts of data using powerful bioinformatics tools, together  
179 with breakthroughs in instrumentation and imaging technology, now allows capturing  
180 molecular processes within structured macroscopic bacterial populations (mm scale) at  
181 near single-cell resolution ( $\mu\text{m}$  scale, (12, 16–18). Multi-scale, high-resolution approaches  
182 leading to high-dimensional readouts based on techniques such as 3D imaging, flow  
183 cytometry and cell sorting, imaging mass spectrometry and single-cell transcriptomics are  
184 now readily available to gain insights into subpopulation structures and the functions of  
185 the individual cell within them (**Figure 2**). But a mechanistic understanding of the  
186 underlying biological processes from the cellular to the population level and finally to the  
187 emerging overarching functions requires tightly linked correlative data analyses by  
188 combining different approaches.

189

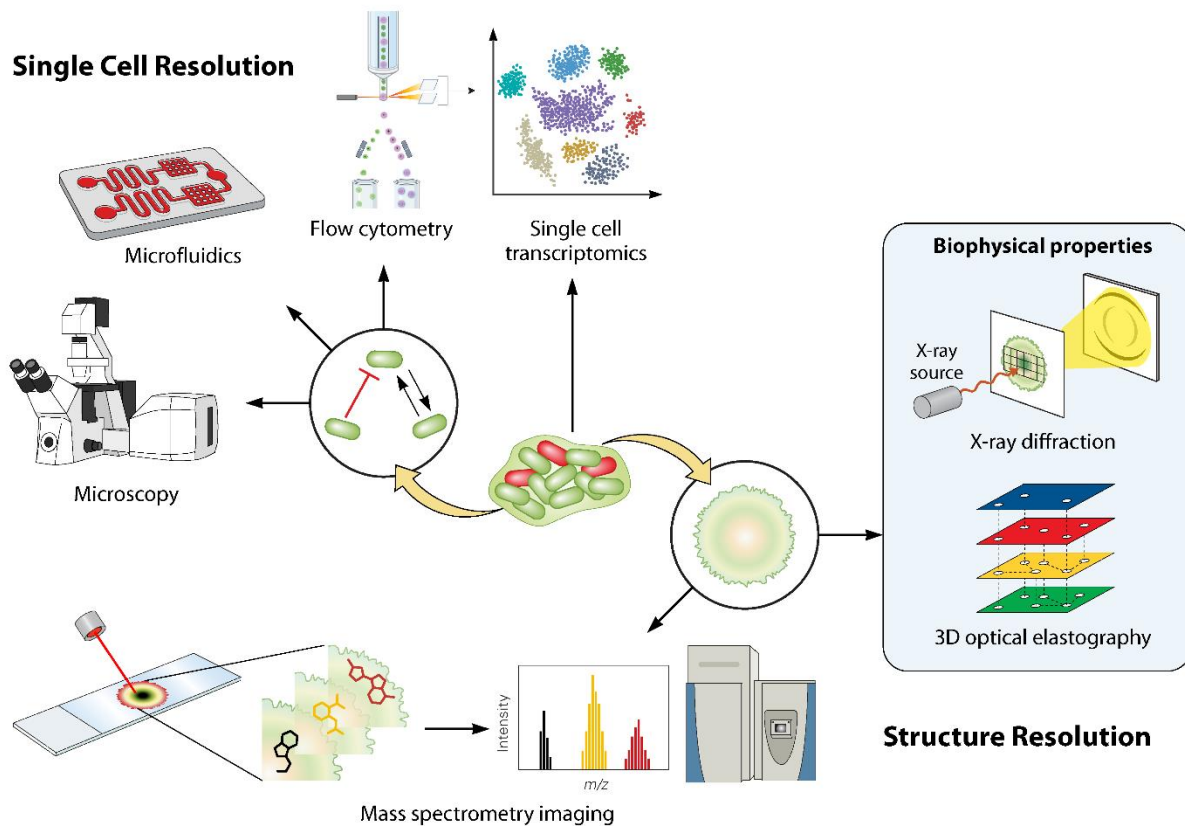


190  
 191 **Figure 1:** Schemes of pure population multicellularity, where divergent functions of  
 192 individuals contribute to overarching functions of the whole population. **A:** Interaction of  
 193 different individual cell types in a colony of *Bacillus subtilis* in response to nutrient scarcity:  
 194 An increasing number of spores can be found in the center of the colony. Near the outer  
 195 edge, some of the cells produce toxins to initiate a suicide mechanism in favor of the  
 196 surviving cells. Swarming cells penetrate to the outer edge of the colony and search for  
 197 new nutrient resources. **B:** Division-of-labor as possibility to fix dinitrogen gas as nitrogen  
 198 source. The photoautotrophic cyanobacterium *Anabaena* sp. develops heterocysts within  
 199 a filamentous chain of cells when facing nitrogen starvation (19). **C:** Resilience to  
 200 perturbation in a *B. subtilis* biofilm after dissection of a part of the colony. Wound healing  
 201 occurred by an initially fast outgrowth of residual cells that remained on the substrate after  
 202 the biofilm piece removal (20).

203

204  
205  
206  
207  
208  
209  
210  
211  
212  
213  
214  
215

This review aims to succinctly summarize available advanced technologies for the analysis of emergent functions of structured multicellular bacterial populations down to the single-cell level. It also discusses the challenges and opportunities associated with studying multicellular bacterial populations using these technologies. The review emphasizes the need to apply high-resolution methods, both at different scales and in combination, to penetrate the complex nature of microbial populations, for example, by elucidating defense mechanisms in response to perturbations, or by elucidating how nutrients are utilized within a structured multicellular population. The technologies discussed aim to, and can, provide a gateway to understanding how each individual cell contributes to the collective action of a confined population.



216  
217  
218  
219  
220  
221

**Figure 2.** Overview of the recent technologies used for the study of multicellularity in bacterial biofilms (greenish and reddish dots represent cells that form a colony). From analyzing population structure to resolving single cells, these techniques are helping to uncover the overarching functions of the entire population.

222 **1. Analysis of spatiotemporal distribution of single cells in intact biofilms by**  
223 **microscopy**

224

225 Analyzing the spatiotemporal distribution of single cells within biofilms through  
226 microscopy provides critical insights into the dynamic organization and interactions of  
227 microbial populations. This section delves into the methodologies employed to achieve  
228 high-resolution imaging and the computational tools used to interpret the complex spatial  
229 and temporal patterns observed within these biofilms.

230

231 Fluorescence microscopy techniques, including single-point-scanning confocal  
232 microscopy, multi-point-scanning confocal microscopy, or selective plane illumination  
233 microscopy, have emerged as important methods for achieving 3D spatial resolution (21–  
234 23). Of particular note is the ability of these microscopy techniques to capture time-  
235 resolved, 3D images of living cells within population structures without significantly  
236 disrupting their behavior. This is made possible by the use of fluorescent proteins that are  
237 fused to proteins of interest, or antibodies conjugated to a fluorescent dye, or fusions of  
238 fluorescent proteins to promoters of interest, which report on the levels of a particular  
239 protein, or the expression of a particular gene. However, the use of fluorescent proteins  
240 and 3D fluorescence microscopy has technical caveats that need to be carefully  
241 evaluated when using this technique. The use of fluorescent protein-based reporters can  
242 alter the biological processes under investigation. Fusions of a protein of interest coupled  
243 to a fluorescent protein may not have the same level of activity as the native protein,  
244 which may modify the biological process under investigation. Similarly, using antibodies  
245 to label a protein of interest may interfere with the function of this protein. Furthermore,  
246 promoter reporters that are supplied on a plasmid may alter the levels of transcriptional  
247 regulators that bind to the promoter of interest at the native chromosomal locus. An  
248 additional issue is that the currently available bright fluorescent proteins require oxygen  
249 for folding into a functional conformation, which severely limits their application in biofilms  
250 above a certain size range, as the center of these biofilms are anaerobic (24). Current  
251 anaerobic fluorescent proteins unfortunately display a low level of brightness. When  
252 performing time-resolved imaging of 3D biofilms using fluorescent proteins, the amount  
253 of laser light that is deposited into the sample usually causes photobleaching of the  
254 fluorescent proteins over time, and may also lead to phototoxicity that alters the biological  
255 processes under investigation (25). However, when the laser exposure is minimized, and  
256 care is taken that the reporters are functional and do not significantly interfere with the  
257 cellular activities, time-resolved 3D imaging of bacterial biofilms using fluorescence  
258 microscopy is a powerful tool for studying the organization and dynamics of these  
259 populations.

260

261 Upon acquisition of fluorescence microscopy images of biofilms with 3D spatial resolution,  
262 potential temporal resolution, and one or more fluorescence channels, the analysis of  
263 bacterial properties in such multidimensional images typically presents challenges (21).  
264 As manual image analysis is typically biased, or even impossible for very large datasets  
265 with millions of images, computational image analysis techniques have been developed  
266 for analyzing bacterial populations. The earliest software solutions performed image  
267 analysis without (or with very limited) spatial resolution inside the biofilms, such as  
268 COMSTAT, COMSTAT2, or PHLIP (26–28). More recent software, such as Daime and  
269 BiofilmQ enable analysis of images with spatial resolution (29, 30).

270  
271 To analyze microscopy images of entire bacterial populations with spatial resolution,  
272 presently, there are two broad options: the first option is relevant when image resolution  
273 is not sufficient to detect individual cells or single-cell analysis is not required, or the  
274 research focus lies on non-cellular entities such as the biofilm matrix. In this case the  
275 software BiofilmQ provides an algorithm that can perform a spatial analysis based on the  
276 dissection of the image of the biofilm population into pseudo-cells with cubical shape (30).  
277 The second option is to detect the individual cells in the population structure, followed by  
278 an analysis of the detected cells and their spatial context. Numerous software solutions,  
279 including BacStalk, Oufiti, the imageJ-based tool MicrobeJ, DeLTA, and SuperSegger,  
280 facilitate the detection of individual cells and intracellular analysis in 2D images, such as  
281 those implemented in (31–35). These tools often also enable the intracellular analysis of  
282 the fluorescent signal distribution within cells. Although detection of bacterial cells in 3D  
283 images have received comparatively less attention, traditional image analysis  
284 methodologies have been established several years ago for coccoid-shaped and rod-  
285 shaped bacterial cells (21, 36, 37). More recently, convolutional neural networks have  
286 strongly improved the detection accuracy of single bacterial cells in 3D (22, 38, 39), with  
287 the adaptation of the StartDist neural network for bacterial cell shapes, termed StarDist  
288 OPP, demonstrating the highest accuracy so far (38). After the detection of the individual  
289 cells in 2D or 3D, or the dissection of low-resolution images into pseudo-cells, BiofilmQ  
290 offers numerous tools for computing spatial relationships between cells and determining  
291 their positioning relative to the biofilm surface, biofilm center, or substrate surface (30).

292  
293 Despite the advances in fluorescence microscopy techniques and image analysis  
294 techniques, fluorescence microscopy-based analysis of bacterial population attributes is  
295 limited. The limited imaging depth that confocal microscopy techniques can achieve,  
296 restricts the analysis to the outer layers of a colony - studies that image single cells in  
297 biofilms loose single-cell resolution at depths beyond approximately 30  $\mu\text{m}$ , due to  
298 scattering of photons in densely-packed bacterial biofilms (21). Even if single-cell  
299 resolution is not required or desired, the optical scattering of photons reduces the signal-  
300 to-background ratio further into the biofilm. Additional imaging depth can be obtained by

301 using two-photon microscopy, but this technique suffers from lower spatial resolution  
302 compared with the widely-used single-photon confocal microscopy techniques.  
303 Additionally, phototoxicity from excitation light, which is particularly relevant for 3D  
304 imaging with confocal and two-photon microscopy techniques, can potentially alter the  
305 natural behavior of the cells. Furthermore, fluorescence microscopy-based analysis is  
306 typically constrained to artificial biofilm setups with a limited number of fluorescent  
307 proteins or fluorescent probes, which may not fully reflect the complexity of even pure  
308 colony biofilms. However, the outlook is promising as ongoing research efforts are  
309 focused on improving advanced microscopy techniques, such as light-sheet microscopy  
310 and adaptive optics, to overcome the imaging depth limitation.

311 Another useful technique is microscopic Raman spectroscopy imaging, which can non-  
312 destructively characterize physiological states of bacterial cells (40). In most cases,  
313 changes in macromolecular composition between cells can be determined, but  
314 biomarkers such as autofluorescent molecules or storage molecules (41) can also be  
315 detected locally in individual bacterial cells. Functional interconnectivity between cells can  
316 be traced using metabolite-linked heavy isotopes by Raman-SIP, although this is currently  
317 mainly performed on community samples where metabolic exchange occurs between  
318 different species (42–44).

319 For all technologies, the integration of machine learning algorithms and the development  
320 of end-to-end automated pipelines for image analysis hold the potential to address the  
321 challenges of accurate segmentation and high-throughput analysis in the future.

322

## 323 **2. Analysis of the spatial distribution of metabolites and structural lipids in** 324 **bacterial colonies and biofilms using mass spectrometry imaging**

325 Microscopy can provide detailed insights into the spatial organization of single cells within  
326 biofilms, but is limited by the requirement of using fluorescence reporters. Mass  
327 spectrometry imaging (MSI) as a label-free technique offers a complementary approach  
328 to analyze the spatial distribution of metabolites and structural lipids within structured  
329 microbial populations (45). MSI builds on the annotation of molecules of interest based  
330 on their mass to charge ( $m/z$ ) ratio as registered by a mass analyzer. This flexibility,  
331 together with a generally high detection sensitivity and the ability to use tandem MS  
332 technologies for further structural characterization and identification are reasons why MS-  
333 based methods serve as primary analysis techniques in several omics-fields, such as  
334 proteomics, metabolomics and lipidomics (46). The most widely used method for imaging  
335 of bacterial metabolites is matrix-assisted laser desorption ionization (MALDI-MSI). With  
336 this technique, samples are coated with a thin film of a “matrix” – a small organic  
337 compound that is absorbing the laser light and assists in transferring thermally labile  
338 biomolecules into the gas phase as well as their ionization. To obtain the information  
339 about the spatial position, the so-prepared samples are scanned with a laser beam on a

340 pixel-by-pixel basis. Typically, this occurs in a vacuum ion source. The mass spectra  
341 registered at the individual positions are evaluated using dedicated software to generate  
342 presentations of the molecular profiles and for further bioinformatic evaluation, such as a  
343 segmentation analysis (47). New developments in MSI instrumentation increasingly  
344 enable a robust single-cell detection level for eukaryotic systems at about 5  $\mu\text{m}$  pixel size  
345 (47, 48). To improve this value to the low micrometer range, MALDI-2 and more recently  
346 transmission-mode (t-)MALDI-2 have been introduced (49, 50).

347 Compared to eukaryotic systems, the analysis of bacterial cultures and biofilms poses  
348 several additional challenges: First, the high rigidity of bacterial cell walls along with their  
349 small cell size require advanced protocols for an efficient extraction of cytoplasmic  
350 compounds (45, 51). Second, the complex composition of bacterial biofilms, consisting of  
351 cells with very different functions and eventually bacterial spores (e.g. for *B. subtilis*  
352 colonies), together with the chemically extraordinarily diverse nature of the extracellular  
353 matrix and excreted signaling compounds, places high demands on any chemical  
354 analysis technique. For the MALDI-MSI analysis, both features are exacerbated by the  
355 need for preserving the spatial information on a meaningful scale, thus to prevent analyte  
356 diffusion across the biofilms.

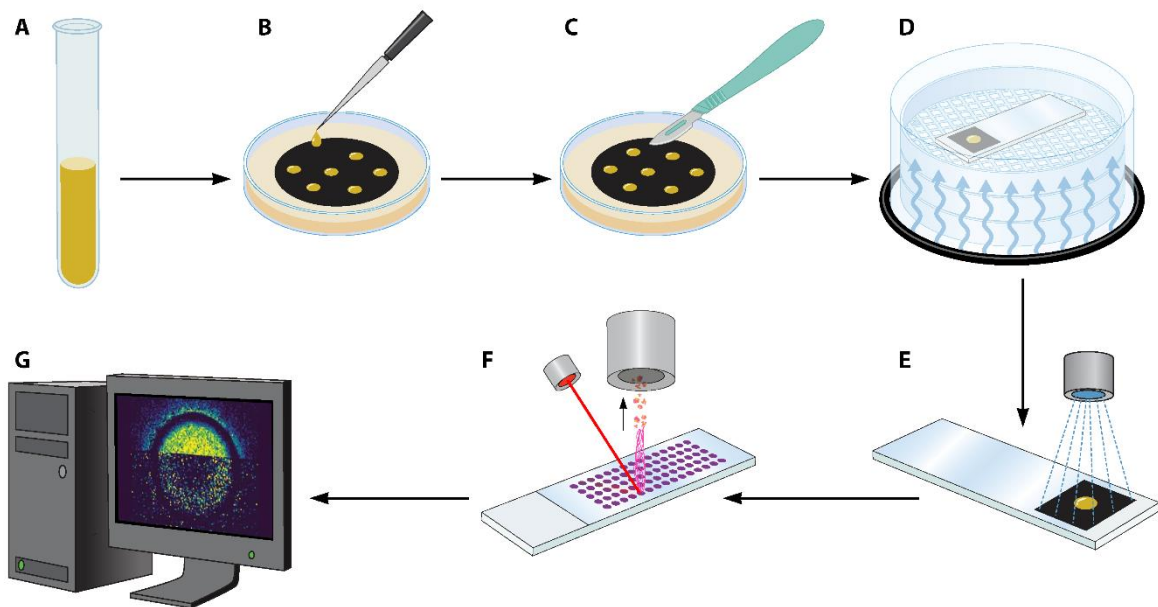
357 As illustrated in **Figure 3**, in most microbial MALDI-MSI studies performed to-date,  
358 biofilms were analyzed in “top view-geometry”, i.e. whole colonies were coated with the  
359 MALDI matrix and the ensemble profiled with the MALDI laser from the front side. A  
360 limitation of this acquisition mode is the averaging effect that is caused by the only poorly  
361 defined extraction of bacterial metabolites from different depths in the sample. To  
362 overcome this restriction, embedding and sectioning protocols similar to those already  
363 established for animal and plant tissue are currently being developed (51, 52). The  
364 combination of optimal sample preparation, high-resolution t-MALDI-2-MSI and its  
365 amendment with further correlative imaging modalities, such as fluorescence microscopy,  
366 could form the basis for a close-to-single-cell resolution also for bacterial ensembles in  
367 the near future.

368 Third, unlike different to MALDI-based biotyping systems that are routinely used in clinical  
369 settings (53, 54), the technically more complex MALDI imaging instruments are typically  
370 not placed in a dedicated microbiology laboratory. To safely inactivate pathogens prior to  
371 the MALDI-MSI analysis, protocols have been developed, in which bacterial biofilms are  
372 grown on filter media, such as mixed cellulose ester membranes (**Figure 3**, 50, 51). At  
373 defined time points, the biofilm-containing membranes can be removed from the agar and  
374 then, for example, be applied to a brief steam inactivation step (51). Alternatively, a brief  
375 chemical fixation, for example with 10% formaldehyde solution to kill heat-resistant  
376 spores, may be applied. While steam inactivation has been found to preserve the general  
377 morphology of the biofilms on a macroscopic level (51), shrinkage by dehydration will

378 need to be taken into account in high-resolution studies of cross-sections. Similarly, the  
379 cross-linking of NH<sub>2</sub> groups (e.g. in bacterial peptides or phosphatidylethanolamines of  
380 the cell walls) is potentially leading to unwanted modifications.

381 By applying the filter membrane-based culturing method and the signal enhancement that  
382 is provided by MALDI-2 laser postionization, more than 30 different 2-alkyl quinolones  
383 and 11 mono- and di-rhamnolipids were visualized from *Pseudomonas aeruginosa*  
384 colonies challenged with co-cultured *Staphylococcus aureus* in a spatially-resolved  
385 manner (51). This result indicates a previously unknown multicellular complexity of the  
386 associated quorum sensing and defense pathways. Other important classes of bacterial  
387 metabolites that have been visualized in this way were *B. subtilis* surfactins and  
388 plipastatins (51). The spatially resolved detection of spore delaying protein (SDP) and  
389 sporulation killing factors (SKF), two endotoxins involved in cannibalism mechanism of *B.*  
390 *subtilis* (55), by MALDI-MSI was previously further correlated with fluorescence  
391 microscopy of a GFP-expressing mutant (56) .

392

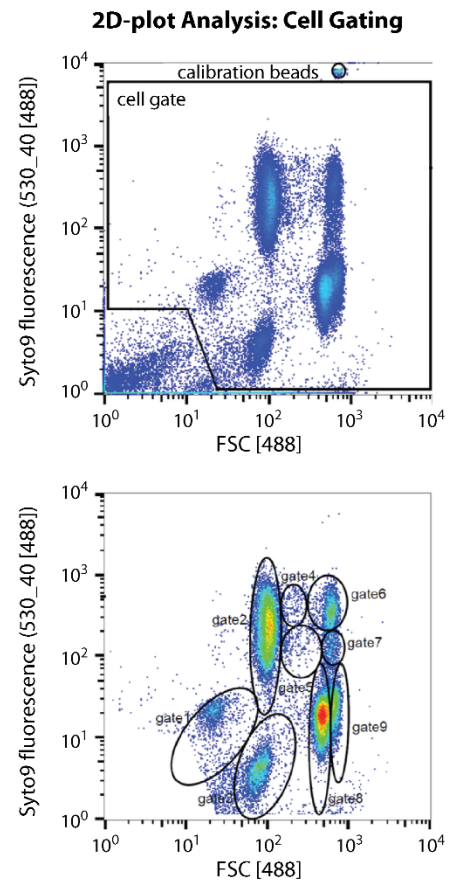
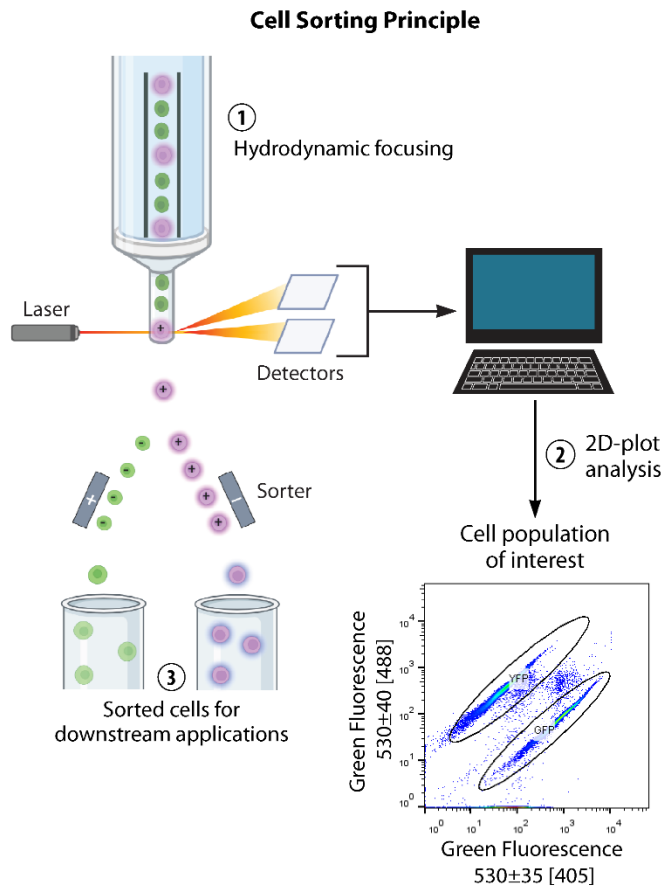


393

394 **Figure 3: Scheme for MALDI-MSI compatible culturing and sample preparation of**  
395 **bacterial colonies for top-view analysis.** **A:** cultivation of cells in LB-broth. **B:**  
396 Inoculation of 1 µL bacterial suspension on a mixed cellulose-ester membrane placed on  
397 LB-agar. **C:** Dissection of a colony together with the membrane. **D:** Optionally: Steam  
398 inactivation. **E:** MALDI matrix coating. **F:** MALDI-MSI experiment. **G:** Data processing.

399 **3. Analysis of single-cell heterogeneity and its local dynamics by microbial flow**  
400 **cytometry**

401 The different molecules detected by MALDI-MSI at specific sites within a colony in situ  
402 are produced by cells that have differentiated into functionally diverse cells. To further  
403 study spatiotemporal variations in phenotypic functions, either a robotic arm can be used  
404 for cell sampling based on phenotypic imaging data (57), or biopsies can be taken from  
405 colony biofilms at different locations for subsequent flow cytometry analysis (58). Flow  
406 cytometry is a powerful method for analyzing bacterial colonies at the single-cell level to  
407 decipher phenotypic heterogeneity. The method is widely used in medical research to  
408 characterize individual eukaryotic cells and is also very powerful for the rapid and  
409 quantitative analysis of individual microbial cells in a high-throughput process (**Figure 4**).  
410 A flow cytometer typically measures between 3,000 to 5,000 cells/sec by aligning cell  
411 after cell in a liquid stream through hydrodynamic focusing. Light scattering is detected at  
412 small angles for forward scattering (FSC) or at 90° for side scattering (SSC), while  
413 fluorescence of the cells is also recorded at 90°. The emitted photons are collected by  
414 photomultipliers and are electronically amplified. Cytometers can have several laser lines  
415 for excitation and are calibrated with bead or cell standards and the obtained data is  
416 commonly displayed in so-called 2D plots, in which two of the measured cell parameters  
417 are visualized (**Figure 4**). Bacterial cells pose a challenge in differentiating cell types due  
418 to their small size, morphological similarity and smaller number of cellular components.  
419 Consequently, flow cytometers used in microbiology require higher resolution due to  
420 lower dye binding and the lack of widely available cell-specific markers, necessitating  
421 customized protocols for each species (59).



422

423 **Figure 4. Flow cytometric analysis of cells obtained from a *B. subtilis* colony.** Left:  
 424 Intrinsic (e.g., scattering) and extrinsic (e.g., fluorescence) parameters of the cells are  
 425 measured by flow cytometry, and the resulting cell subsets are displayed as a 2D plot.  
 426 From here, a sorting decision is made and the cells are sorted by FACS (fluorescence  
 427 activated cell sorting) accordingly for subsequent analysis. Right: *B. subtilis* cells are  
 428 characterized with FSC and Syto9 staining (for nucleic acids). The population diversifies  
 429 into several heterogeneous subpopulations with different vegetative cell types and spore  
 430 types. Top, a cell gate is set to separate cells from all other events. Bottom, cell  
 431 distributions are shown without instrumental noise and calibration beads. Each  
 432 subpopulation is separated from the others by gating for both cell number determination  
 433 and cell sorting. The colors from blue to red indicate the increasing number of cells per  
 434 subgroup of cells.

435 The assessment of cellular characteristics can be achieved through intrinsic or extrinsic  
 436 parameters. Intrinsic parameters do not require cell treatment and convey light scattering  
 437 properties, using both forward scattering, which provides information about cell size, and  
 438 side scattering to measure cell density and surface roughness (60).

439 Gene expression can be quantitatively visualized using fluorescent reporter gene fusions  
440 (16). Additionally, autofluorescent pigments in autotrophic cells (61) or fluorescent marker  
441 molecules of metabolic pathways (62) identify cell types and quantify metabolic activities.  
442 The advantage of analyzing intrinsic parameters lies in the ability to assess cells without  
443 altering their physiological state. On the other hand, extrinsic methods involve labeling  
444 cell functions using fluorescent dyes, such as functional FISH probes or antibodies,  
445 although these labels may not always be quantitative due to non-penetrable cell walls  
446 (63). These methods can also measure viability states (e.g. live/dead ratio, membrane  
447 potential, pH (64) or quantify cellular macromolecular components such as protein or DNA  
448 levels (65). Despite the large number of fluorescent markers available, only two or three  
449 dyes can be simultaneously applied to a single bacterial cell to avoid (or not to disturb)  
450 phenomena like fluorescence resonance energy transfer or compensation depletion (66)

451 Flow cytometry is often used to accurately quantify absolute cell numbers in  
452 microbiological populations. A recent study examined wound healing in *B. subtilis*  
453 colonies, where flow cytometry was used to measure fractions of live and dead cells, after  
454 a quarter of a biofilm was removed and compared to normally growing biofilms (20). A  
455 remarkable finding was that cell growth in the biofilm “wound” initially outpaced normal  
456 growth but then later lagged behind due nutrient depletion (see scheme **Figure 1C**). This  
457 initial rapid growth was attributed to residual cells remaining in or on the agar (up to 10%  
458 of the cells) that was overlooked in optical microscopy-based studies. In addition to  
459 analyzing live and dead cells, also various cell cycle states can be differentiated. The  
460 dynamics of heterogeneous cell types and proportions can be tracked over time, providing  
461 a complex view of spatially and temporally coherent physiological processes in bacterial  
462 populations. An example for dynamic cytometric fingerprinting of growth-related cell  
463 states is shown for *Prestia megaterium* in SI MOVIE 1. Furthermore, fluorescent reporters  
464 can be used to study the broad functional behavior of cells in pure populations (67, 68).  
465 Interestingly, in the absence of reporter genes or functional fluorescent dyes, functional  
466 diversity can also be identified using correlation analysis by combining cell information  
467 (coming from flow cytometry) and cultivation related abiotic parameters. The associated  
468 different cell types and abiotic factors, including measurable gradients of oxygen or  
469 carbon and energy sources, as well as synthesized macromolecules such lipopeptides  
470 (e.g. surfactants and plipastatins in the case of *B. subtilis* and 2-alkyl-quinolones and  
471 mono- and dirhamnolipids for *P. aeruginosa*, (51)) could serve to estimate the cell-cell  
472 and cell-abiotic interactions. In addition, the strength of correlations between cell types as  
473 well as cell types and abiotic factors can be used for sorting decisions. The 2D data  
474 generated by flow cytometry can be automatically gated using the tools PhenoGMM (69)  
475 and flowEMMi (70) or evaluated and visualized by flowCHIC (71), flowCybar (72, 73) or  
476 Flowsofine (74).

477 The potential of flow cytometry is greatly enhanced by its ability to separate cell types  
478 locally by cell sorting (FACS - fluorescence activated cell sorting). Functions of sorted  
479 subpopulations can then be identified in detail by subsequent omics technologies such  
480 as proteomics (75, 76), or transcriptomics (77, 78). A pioneering study that applied  
481 proteomics analysis on sorted bacterial cells revealed the differences in protein  
482 compositions of *E. coli* and *P. putida* strains (79). Such cell separation techniques can  
483 provide insight into the interactions between cell types and, by excluding unsorted cells,  
484 facilitate the identification of protein biomarkers and protein-protein interactions  
485 associated only within the sorted cell phenotypes (76, 80). Additionally, recent  
486 advancements in sequencing technologies, including single-cell RNA-seq, permits  
487 targeting single cells for functional assessment and facilitating the identification of various  
488 functional subgroups in bacterial colonies (81, 82). Although very promising, these  
489 methods are still limited by the structure of prokaryotic cells, which may cause higher  
490 sequencing costs and detect low numbers of transcripts with higher uncertainties (78, 83,  
491 84). Alternatively, the prior sorting of bacterial subpopulation by FACS, coupled with  
492 traditional bulk mRNA-seq analysis, can generate high precision gene expression profiles  
493 of cell subgroups (77). In addition, vital cells with certain physiological properties can be  
494 sorted for further cultivation approaches or specific viability tests (85). Nevertheless, there  
495 are still limitations when performing cell sorting on bacterial single cells or relatively small  
496 numbers of cells, especially if subsequent omics applications are to be conducted. It is  
497 also important to note that, unlike live cell imaging, e.g. in microfluidic devices, individual  
498 cells cannot be tracked over time.

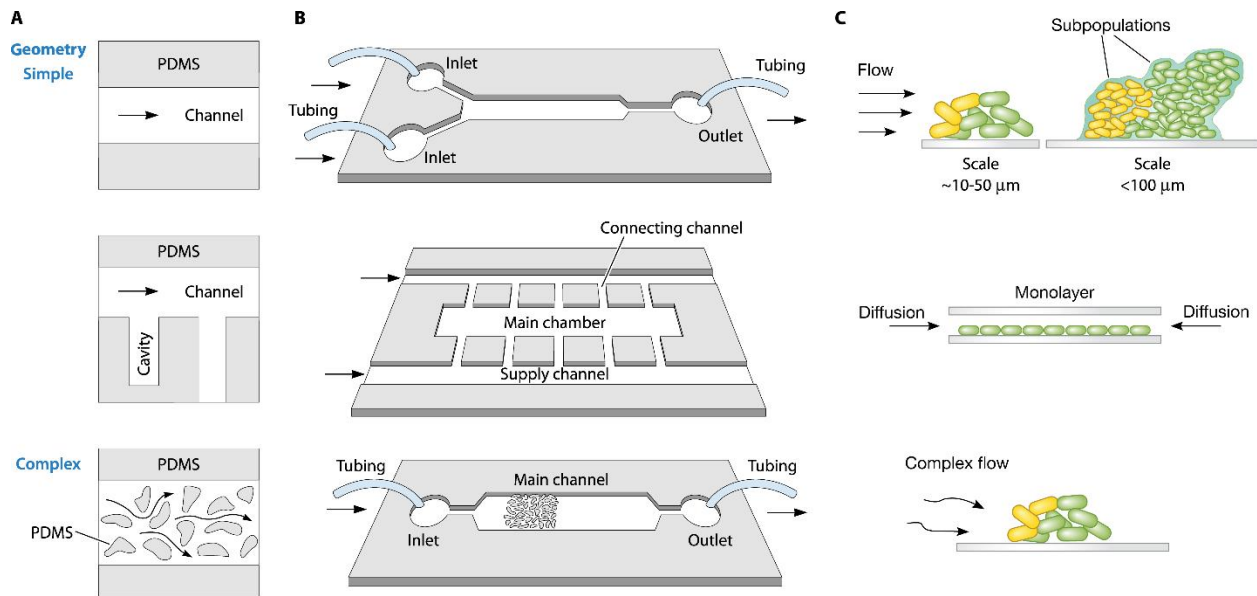
499

#### 500 **4. Analysis of early biofilm development and behavior by microfluidic cultivation** 501 **systems**

502 Microfluidics deals with the handling and control of fluids on the micrometer scale (86, 87)  
503 and is therefore an ideal tool for analyzing microbial biofilm development in a well-  
504 controlled environment. Established microfabrication techniques employing soft  
505 lithography and replica molding (88, 89), as well as emerging 3D-printing (90–92) allow  
506 the generation of channels with lower micrometric features. These features may range  
507 from simple straight channels to various complex geometries (**Figure 5A, B**). Within the  
508 microfluidic channels, well-controlled, stable and reproducible environments can be  
509 established and maintained. Controllable environmental parameters are for instance the  
510 composition of the medium, its flow speed, chemical gradients and if applicable, the  
511 ambient temperature. The use of transparent materials such as polydimethylsiloxane  
512 (PDMS) and glass enables the integration of microfluidic devices with optical methods for  
513 readout, such as life-cell imaging and high-resolution microscopy. The resulting spatial  
514 and temporal resolution of the recordings are precise enough to track individual cells

515 within a cell cluster or even smaller biofilms and thus monitoring growth, cell division and  
516 fluorescence coupled metabolic parameters (21, 36). Both large-scale imaging of  
517 developing biofilms and recording of small cell clusters require an integration of  
518 microfluidics with automated high-resolution microscopy image acquisition and will  
519 benefit from advanced imaging methods such as confocal laser scanning microscopy.

520 Various microfluidic systems have been developed to investigate and characterize  
521 biofilms (93, 94). Naturally, the unbounded growth of a bacterial biofilm is best studied in  
522 a straight, large aspect ratio microfluidic channel (36, 95) (**Figure 5 A-B top**). This  
523 maximizes the observable area and avoids unnecessary complex flow profiles. While a  
524 straight channel is a simple geometry, the flow may still be tightly controlled by the  
525 integration of multiple inlets (96, 97). Defined flow conditions allow to determine the  
526 impact of the medium and molecules of interest, such as for instance antibiotics, on biofilm  
527 formation (98, 99). The flow itself may be characterized experimentally by employing and  
528 tracking fluorescent tracers, or numerically through computational fluid dynamics (100–  
529 102). In nature, a bacterial biofilm is often opposed to a dynamic environment, defined by  
530 changing shear forces (103–105). The impact of flow shear on bacterial adhesion, onset  
531 of biofilm formation and subsequent development can be investigated in microfluidic  
532 devices in a defined manner (106). Furthermore, the chemical composition of the biofilm  
533 surrounding medium may also change dynamically. Over the years, microfluidic assays  
534 were developed to overcome the limitations posed by static biofilm methods and are  
535 capable of tracing the physiological response of bacterial populations to well defined  
536 chemically fluctuating environments (107–109). Finally, the architectures of natural  
537 environments are inherently complex and heterogeneous (110, 111). These  
538 heterogeneities can be modeled using microfluidic devices and their micrometer  
539 resolution. For instance, the cavity-like pores of the human skin and mammalian gut  
540 surface (112) were simulated by creating microfluidic cavities (107, 113, 114), **Figure 5**  
541 **A-B middle**). Similarly but even more complex, soil as a habitat of water, air and particles  
542 of varying length scales was recently mimicked in microfluidic channels using small  
543 diameter circular PDMS pillars or even fully heterogeneous PDMS structures (115–117)  
544 **Figure A-B bottom**).



545

546 **Figure 5. Overview of a microfluidic approach to biofilm analysis.** **A:** The  
 547 microfabrication process allows for a large variety of channel geometries. Three  
 548 exemplary geometries representing a straight channel (top), a microfluidic cultivation  
 549 chamber with dead end or open cavities (middle) and a complex soil like geometry  
 550 (bottom) are shown. **B:** Respective examples of such geometries. A wide aspect ratio  
 551 channel with multiple inlets (top), a microfluidic cultivation chamber (middle), a  
 552 microfluidic channel with irregularly shaped obstacles (bottom) (see (97, 118, 119) for  
 553 more details). In general, one or more syringe pumps drive a fluid flow (black arrows)  
 554 through the microfluidic channel(s) and connected tubing. **C:** Sketched examples of  
 555 different biofilm growth and experimental conditions regarding the respective microfluidic  
 556 approaches. The growth and development of bacterial biofilms, and potentially also  
 557 fluorescently labeled subpopulations (yellow, green) therein, can be studied from single  
 558 or few cells up to small biofilms of several 10,000 cells.

559 Microfluidic systems have improved the understanding of the mechanisms underlying  
 560 biofilm formation and early biofilm development. They provide a useful tool for  
 561 investigating the dynamic interactions within the biofilm structure and function, its  
 562 composition and the external environment, determined by the applied flow, medium and  
 563 surrounding geometry. Ultimately, natural microbial biofilms exhibit significant  
 564 heterogeneities themselves, often comprising diverse species or genotypes in dynamic  
 565 environments (120). In contrast to well mixed scenarios, the fundamental evolutionary  
 566 forces of genetic drift and selection may be altered in a bacterial biofilm (121, 122). In  
 567 conjunction with automated microscopy and lineage tracing, such heterogeneities may  
 568 be introduced into a microfluidic grown biofilm by pre-mixing fluorescently labeled bacteria  
 569 with a pre-determined fitness difference. Naturally, a multitude of different microcolonies  
 570 and biofilms with varying fractions of two genotypes will be present and their growth and

571 development can be recorded (**Figure 5C**). For instance, (123) described the biphasic  
572 competitive dynamics between *E. coli* strains with and without a growth rate difference in  
573 microchannels. Furthermore, the potential of microfluidics to create micrometric features  
574 was used to characterize the colonization resistance of packed bacterial populations in  
575 small cavities (113) and, more recently, to demonstrate the impact of the local cavity  
576 geometry on the evolutionary fixation probability (114). Another recent study examined  
577 the dynamics of polarization at different stages of colony development by using  
578 microfluidic flow chambers in combination with microscopy and fluorescence single-cell  
579 analyses. It was found that hyperpolarization emerges at the colony center and  
580 progresses outward to the periphery, which marks a transition to collective membrane  
581 potential dynamics (124) that is associated with the growth resources and oxygen  
582 concentration.

583 In the last few years, several microfluidic single-cell cultivation devices, based on ‘mother  
584 machine’ like micro-chemostats (95, 125) have been developed. These enable the  
585 analysis of single cells and small cell clusters with full spatiotemporal resolution (126).  
586 Furthermore, microfluidic monolayer growth chambers allowed investigating various  
587 biofilm-related aspects, such as the onset of biofilm formation in *B. subtilis* at single-cell  
588 level (118, 127). While a closed system is paramount for a stringent environmental control  
589 and long-term operation, it opposes the selective sampling of cells or subpopulations.  
590 Recently, this was overcome by integrating a robot-assisted sampling device, which  
591 pierces the PDMS above and subsequently samples from the microfluidic channel below  
592 in a pre-defined manner (128, 129). This approach would allow integrating e.g. FACS-  
593 sorting and single-cell transcriptomics, as described in the next chapter.

594 A potential limitation during long term operation is the formation of large clumps by non-  
595 adhering bacteria and/or flow induced shedding of extracellular matrix (130). This may  
596 ultimately clog the inlet, outlet or main channel and thus alter or even fully stall the applied  
597 flow. To prevent clogging the experiment may require the application of undesirably high  
598 flow rates and thus shear stress. Biofilm experiments employing microfluidic channels  
599 usually focus on relatively small but well-resolvable biofilms. Probing the properties of  
600 large biofilms (millimeter scale) regarding gene expression profiles, 3D structure,  
601 mechanical stiffness, cell density, etc. therefore need to be studied with a different set of  
602 methods.

603

## 604 **5. Analysis of cellular function in single cells: Single-cell transcriptomics**

605 It has long been recognized that isogenic bacterial populations can exhibit a significant  
606 phenotypic diversification, e.g. under specific stimuli (131). Thus, microbial populations  
607 exhibit intricate structures and nutrient gradients resulting in the emergence of locally

608 distinct subpopulations (132). While traditional methods, such as the already mentioned  
609 FACS and microscopy help quantifying cell phenotypes, these and other techniques fail  
610 to capture the full spectrum of bacterial behavior within biofilms. This limitation can now  
611 be overcome with omics technologies. RNA sequencing (RNA-seq) has proven to be a  
612 powerful tool to capture the full spectrum of bacterial physiology, but has mainly been  
613 applied in approaches averaging the signal over millions of bacteria (133). Yet, a new  
614 generation of technologies has emerged in 2020 to capture the transcriptome of single  
615 bacteria. Such approaches hold immense promise for revolutionizing our knowledge of  
616 biofilm dynamics. The following sections discuss the variety of the different protocols and  
617 the challenges associated with implementing such emerging protocols.

### 618 **5.1. Challenges associated with capturing the RNA of a single bacterium**

619 Single-cell RNA-seq (sc-RNA-seq) approaches have become a standard application in  
620 eukaryotic molecular biology (134). Adapting these techniques to bacterial systems must  
621 take the molecular, physiological and morphological differences into account. Bacterial  
622 cells contain only around 1/100 of the total RNA of an eukaryotic cell (78), the average  
623 half-life of bacterial mRNAs is often only in the range of seconds to a few minutes in  
624 contrast to the minute-to-hours range of eukaryotic cells (135–138) and mRNA  
625 enrichment via poly-A tails is not directly possible in bacteria. Moreover, there is no  
626 universal lysis method that works at the single-cell level and usually conditions must be  
627 adjusted for each bacterial species (139). Another obstacle is the isolation of single cells  
628 from multicellular bacteria, such as *Anabaena* and *Nostoc* species, which grow in one-  
629 dimensional filaments covered by a robust cell wall and sheath, have a periplasm  
630 continuous along the entire filament length (140) and are connected by a particular type  
631 of prokaryotic gap junctions (141). There are multiple protocols for the isolation of mature  
632 heterocysts from these filaments (142, 143). These protocols have been successfully  
633 used for the separation of heterocysts and vegetative cells with the objective of  
634 investigating their respective transcriptomes using microarrays (144).

635 To summarize, several approaches have been developed for bacterial single-cell  
636 transcriptomic analysis to overcome these different roadblocks (see below and **Table 1**).  
637 Beyond these general bacterial challenges, studying bacteria within biofilms at a single-  
638 cell resolution adds additional complexities: i) Biofilms are densely packed populations  
639 encased in an extracellular matrix, which itself is a physical barrier to access all members  
640 of a population (145), ii) Variation in oxygen and nutrient concentration can result in a  
641 myriad of metabolic changes and capturing the full spectrum of these behaviors can be  
642 challenging without the proper techniques to resolve single-cell dynamics (146), iii) The  
643 different growth stages of a cell within the biofilm life cycle is dynamic and capturing the  
644 transcriptome of attachment, expansion, maturation and dispersion states might be  
645 essential for elucidating the temporal gene expression patterns and regulatory  
646 mechanisms driving the complex behaviors exhibited by bacteria within biofilms (147).

647 Considering the challenges of just performing transcriptome studies in bacteria alone, it  
648 has been a major achievement that single-cell transcriptomics has been successfully  
649 established in the biofilm context. In the next section, the latest advancements of sc-RNA-  
650 seq in bacteria and their applications are described.

## 651 **5.2. Single-bacteria RNA-seq using combinatorial methods**

652 Split Pool Ligation-based Transcriptome sequencing (SPLiT-seq) was originally  
653 developed for eukaryotic single cells (148) and was then adapted for bacterial cells  
654 (*Escherichia coli* and *B. subtilis*) leading to the microbial split-pool ligation-based  
655 transcriptomics (microSPLiT) and prokaryotic expression profiling by tagging RNA in situ  
656 and sequencing (PETRI-seq) (149) protocols. These methods do not require the prior  
657 isolation of single cells. Instead, cells fixed with formaldehyde are distributed into  
658 individual wells, permeabilized and subjected to in situ combinatorial indexing. For this,  
659 cells are split three times across 96-well plates for three rounds of barcoding by reverse  
660 transcription and two ligations (149). In the first step, reverse transcription is primed with  
661 barcoded random hexamer primers specific to each well. For the following two steps, cells  
662 are pooled and redistributed across new microplates for two rounds of barcoding by  
663 ligating another set of barcoded primers to the cDNA. Alternatively, the RNA was  
664 polyadenylated with *E. coli* poly(A) polymerase I and reverse transcribed *in situ* using bar-  
665 coded oligo(dT)-primers (150). Finally, the cells are pooled, lysed, cDNA libraries  
666 prepared and sequenced. In this way, the transcripts of every single cell finally carry a  
667 unique combination of barcodes and therefore can be assigned to individual cells. 5'-  
668 phosphate-dependent exonuclease was used to remove rRNA contaminations.  
669 Additionally, RNase H was used to digest rRNA after reverse transcription primed by  
670 rRNA-specific oligonucleotides (150). In a recent publication, the PETRI-seq protocol was  
671 modified through the depletion of rRNA-derived cDNA fragments through hybridization to  
672 a set of DNA probes resulting in a significant reduction in the fraction of uninformative  
673 rRNA reads from ~96-90% to 46-8% (151).

674 These methods have been used to identify cell-specific expression patterns that would  
675 not have been accessible by bulk sequencing. In the PETRI-seq approach (149), different  
676 populations of *E. coli* and *S. aureus* were sequenced and rare subpopulations exhibiting  
677 distinct gene expression programs were detected (149). Using a modified version of the  
678 PETRI-seq protocol, a small number of cells were identified at the bottom of a static *E.*  
679 *coli* biofilm that expressed the gene encoding Pdel, predicted as a phosphodiesterase  
680 (151). However, the authors demonstrated that the expression of Pdel rather correlated  
681 with elevated levels of the second messenger c-di-GMP and that this effect was  
682 associated with the formation of ampicillin-resistant persister cells (151). Recently the  
683 PETRI-seq approach was used to propose a new classification of regulation based on  
684 measuring the transcriptional response of each gene in individual cells of *S. aureus* and

685 *E. coli* following its replication (152). These combinatorial approaches are limited by the  
686 higher number of cells that are needed to achieve an optimal mRNA capture efficiency.

### 687 **5.3. Single-bacteria RNA-seq on plates**

688 MATQ-seq was also originally developed for single-cell sequencing of total RNA from  
689 eukaryotic cells (153). In the implementation for bacterial cells, single bacteria are sorted  
690 into the wells of a 96-well plate using FACS followed by cell lysis and cDNA synthesis  
691 and amplification(154). The authors used RNAlater to maintain the RNA integrity during  
692 the sorting step. To avoid domination of the resulting cDNA libraries by rRNA- and tRNA-  
693 reads, a more efficient, Cas9-dependent rRNA depletion step was integrated in an  
694 improved version of this protocol, yielding much higher numbers of non-rRNA reads (155).  
695 By this approach, all classes of different bacterial transcripts were detected and the  
696 sensitivity should allow the identification of low-abundance transcripts by MATQ-seq (154,  
697 155). If the approach is combined with a suitable technique to isolate cells in a  
698 reproducible way from a microbial population, it is in principle suitable for analyzing  
699 biofilms at high resolution and high sensitivity. Reproducibility and high sequencing depth  
700 per cell are achieved in plate-based methods, however the number of cells that can be  
701 multiplexed simultaneously is limited to just a few hundreds of cells.

### 702 **5.4. Single-bacteria RNA-seq in droplets**

703 The M3-seq approach combines plate-based, *in situ* indexing with droplet-based indexing  
704 and post hoc rRNA depletion, that is, using RNase H and rRNA-specific DNA probes after  
705 cDNA synthesis (156). M3-seq allows transcriptome-scale sc-RNA-seq at higher cell  
706 numbers and across multiple conditions (156). Another recently developed droplet-based  
707 method has been called BacDrop (84). This workflow involves fixation and  
708 permeabilization of cells followed by rRNA and gDNA depletion before reverse  
709 transcription and indexing using RNase H and DNase I. The first barcoding is performed  
710 during the reverse transcription and the resulting cDNA is polyadenylated at the 3' end  
711 using terminal transferase. The second barcoding then is part of the 2nd strand cDNA  
712 synthesis within droplets. BacDrop was tested on several species, including the gram-  
713 positive *Enterococcus faecium* for broader applicability and indicated heterogeneity within  
714 the investigated bacterial populations (84). While this droplet-based approach provides a  
715 higher throughput power of multiplexing, it requires lab to lab optimization of the available  
716 protocol, which challenges reproducibility.

### 717 **5.5. Spatial transcriptomics for bacteria**

718 An aspect of particular relevance to the study of bacterial biofilms is the assignment of an  
719 obtained transcriptome profile not only to a single cell, but to a specific cell, located at a  
720 distinct position within the respective microbial population. Par-seqFISH is an approach  
721 connecting gene expression and spatial context at single-cell and single-molecule

722 resolution (157). This method was developed from a seqFISH approach targeting  
723 individual cells within the neural crest stem cell niche of chicken embryos (158). The  
724 authors addressed about 600,000 *P. aeruginosa* cells across multiple conditions, in  
725 planktonic and biofilm cultures (157). The mRNAs were hybridized by two sets of probes.  
726 First, a set of 12 to 20 non-fluorescent probes was used. In this approach, all probes  
727 targeting the same mRNA carry identical sequence tags that in a second hybridization  
728 interact with short, fluorescently labeled oligonucleotides called “readout” probes.  
729 Therefore, multiple mRNAs can be detected at once using readout probes labeled with  
730 different fluorophores. The pattern is detected using automated microscopy, then these  
731 probes are stripped and washed away, so the cycle can be repeated, measuring mRNA  
732 levels by a new set of readout probes. The authors used a library of probes targeting 105  
733 marker genes (157). Once the sequential hybridizations were completed, the resulting  
734 images could be combined into spatially resolved multigene profiles at the single-cell  
735 level. Analyzing planktonic and biofilm populations of *P. aeruginosa* by Par-seqFISH, Dar  
736 et al. (157) showed that different transcriptional states emerged dynamically during the  
737 development of a biofilm as well as during planktonic growth, an insight that would have  
738 been impossible to obtain by more traditional approaches. The authors detected 20  
739 different subpopulations with likely different metabolic capabilities and involving the  
740 differential expression of virulence-related genes (157).

741 This technique is very attractive for the characterization of cells in a microbial biofilm. It  
742 can be adapted to different species and conditions, but appears to be technically more  
743 demanding. A certain limitation arises from the fact that only mRNAs can be detected, for  
744 which probe sets were predesigned.

745 This overview summarizes the different approaches for single cell isolation, fixation,  
746 treatment and sequencing from which the most suitable protocol for a given project can  
747 be derived. One should notice, however, that all methods were tested on a very narrow  
748 set of model species (**Table 1**). Therefore, it is important to expand the taxonomic breadth  
749 of bacteria chosen for single-cell transcriptome analysis and to ultimately also aim at more  
750 heterogeneous microbial populations.

751

752

753

754

755

756

757 **Table 1.** Comparison of different approaches developed for single-cell RNA sequencing.

Method	par-seqFISH	SPLiT-Seq (microSPLiT)	PETRI-Seq	MATQ-seq	M3-seq	BacDrop
<b>Cell fixation</b>	Paraform-aldehyde	Formaldehyde	Form-aldehyde	RNAlater	Form-aldehyde	Formaldehyde
<b>Bacteria</b>	<i>P. aeruginosa</i>	<i>E. coli, B. subtilis</i>	<i>E. coli, S. aureus</i>	<i>S. enterica, P. aeruginosa</i>	<i>B. subtilis, E. coli</i>	<i>K. pneumoniae, E. coli, P. aeruginosa, E. faecium</i>
<b>Ribosomal RNA</b>	16S rRNA signals used as reference. Potential for assigning taxonomic information.	Degradation of rRNA by terminator exonuclease and RNase H.	No depletion for rRNA, leading to 84.9% ( <i>E. coli</i> ) and 75% ( <i>S. aureus</i> ) rRNA reads.	DASH for efficient rRNA depletion.	Depletion of rRNA after library amplification using RNase H.	Depletion from total RNA using RNase H.
<b>Advantages</b>	Transcriptome information is assigned to individual cells at spatial resolution.	Microfluidics-independent.	Microfluidics-independent, rare sub-populations of cells detectable.	Sensitivity, rare transcripts detectable. No limitation in sequencing depth.	High throughput and high cell numbers possible.	10x Genomics platform is used.
<b>Technical hallmarks</b>	Parallel hybridization of probes over sequential cycles <i>in situ</i> .	Polyadenylation of mRNAs, combinatorial barcoding over 3 to 4 cycles of adapter ligations.	RT using barcoded random hexamers, combinatorial barcoding over 2 cycles.	FACS-sorting, sensitive RT protocol.	10x Genomics microfluidic droplets.	Droplet- based, enabling use of the 10x Genomics platform.
<b>Suitability for analysis of clonal biofilm populations</b>	Excellent, but limitation in the number of detectable genes because a set of pre- signed probes is needed.	Assignment to a specific cell at spatial resolution is not possible.	No spatial information possible.	Potential for high resolution and high sensitivity analysis if cells are tracked.	Potential if cells are tracked.	Potential if cells are tracked.
<b>Limitations</b>	Limited by number of probes used			Low throughput protocol (100s of cells profile at once)	Not enough sequencing depth achieved. High number of cells required to perform protocol and rare subpopulations might not be captured.	
<b>Reference</b>	(157)	(150)	(149)	(154, 155)	(156)	(84)

758

759

## 760 **6. Analysis of biophysical properties of intact biofilm populations**

761  
762 As was mentioned above, alternating gene expression patterns lead to heterogeneous  
763 distribution of cell phenotypes in biofilms. Locally guiding the formation of biochemical  
764 microenvironments, these processes may then be accompanied by gradients of  
765 biophysical cues such as accumulation of mechanical and osmotic stresses (159, 160),  
766 active cellular processes (161), varying water content and state (162) as well as  
767 hierarchical molecular organization across multiple space- and time-scales (163). Indeed,  
768 a bilateral feedback of mechanical stresses and biochemical patterning is now recognized  
769 to be essential for understanding proper embryonic development of eukaryotes (164).  
770 Similarly, following the close analogy of biofilms to multicellular organisms (165, 166),  
771 proper characterization of biofilm mechanical properties and the reciprocal effect of  
772 molecular gradients and forces currently comes into the spotlight (167).

773  
774 Bacteria in colony biofilms embed themselves in a polymer meshwork, composed of  
775 secreted polysaccharides and fiber-forming proteins, including polysaccharide-binding  
776 proteins, proteases, and nucleases (168). The formation of this extracellular matrix is a  
777 dynamic process, affecting biofilm mechanical properties on the cellular and bulk scales  
778 and as a result its composition varies with spatial position in the biofilm and during biofilm  
779 development (169). To understand biofilm development as a whole, it would be necessary  
780 to view biofilms as composite materials and solve the central puzzle of material scientists,  
781 namely how cells and molecular structures organize to form the complex soft biofilm  
782 material.

783  
784 To determine the density and shape of biofilm colonies optical coherence tomography  
785 (170) can be used. However, specific tools are needed to both quantify material properties  
786 in biofilms with spatial resolution, while also getting insights on the underlying microscopic  
787 structure. The spectrum of biofilm material properties changes from soft colonies grown  
788 on catheters to stiff calcified biofilms on the teeth surface. There is a broad range of  
789 methods to probe viscoelastic properties of biofilms at different scales (171, 172). These  
790 range from standard rotational rheometers, which require large amounts of biomass  
791 (often multiple colonies) (173, 174), to atomic force microscopy (AFM), which provides  
792 spatial resolution of mechanical properties down to the nm scale, but with low throughput.  
793 AFM measurements are also limited by complex interactions of the AFM probe with the  
794 biofilm surface and thus often performed under non-physiological dry conditions or via  
795 ethanol immersion (or other solutions, e.g. NaCl) (175). Bridging the gap between the  
796 macroscopic scale of the entire biofilm and the cellular and molecular scales has been  
797 achieved by fluorescence microscopy techniques that image biofilms at subcellular  
798 resolution, and by 2D electron or X-ray microscopy, which scans large areas with beam  
799 sizes on the order of molecules. Methods, such as transmission electron microscopy and

800 micro-computed tomography (using X-rays) may both be expanded to 3D mapping via  
801 reconstruction of 2D images (tomography). But despite the 3D visualization, the spatial  
802 resolution of these methods still falls behind electron or X-ray diffraction techniques.

803  
804 How to better accomplish high resolution mapping of biofilms in a space- and time-  
805 resolved manner will be discussed in this subsection. The focus will be on fluorescence  
806 microscopy-base rheological measurements (176), a newly developed optical  
807 elastography approach (177, 178) and hierarchical structural analysis with X-ray  
808 diffraction and X-ray fluorescence techniques (163, 179, 180) with the latter two allowing  
809 for label-free, whole biofilm measurements.

### 810 **6.1 Fluorescence microscopy-based microrheology**

811 Given the benefits of fluorescence microscopy techniques for 3D live-cell imaging across  
812 multiple length scales, several techniques have been developed to determine spatially-  
813 resolved mechanical properties of biofilms using fluorescence microscopy. Early  
814 implementations have relied on introducing micron-sized beads into the biofilms, which  
815 can then be tracked using microscopy and image analysis. By following the passive  
816 diffusion of the beads (181–183), or by actively actuating magnetic beads inside biofilms  
817 using a magnetic tweezer (184, 185), the local rheology around the beads can be studied.  
818 However, bacterial cells are expected to be anchored differently to the extracellular matrix  
819 within biofilms than micron-sized beads that were introduced artificially. Therefore, further  
820 approaches have been developed to use the bacterial cells themselves as tracers for  
821 studying the local mechanical properties of biofilms (176, 186). Individual cells are tracked  
822 using microscopy and image analysis, while the biofilm is perturbed by an external stress,  
823 such as strong shear flow (**Figure 6A**). By tracking all cells in biofilms before, during, and  
824 after the mechanical perturbation, it was possible to obtain a map of the elastic modulus  
825 of 3D biofilms with micron-scale spatial resolution (176). Interestingly, the spatial  
826 distribution of the elastic modulus was found to match the spatial distribution of the  
827 polysaccharide component of the extracellular matrix, whereas the other matrix  
828 components did not display a spatial distribution matching that of the elastic modulus.

829

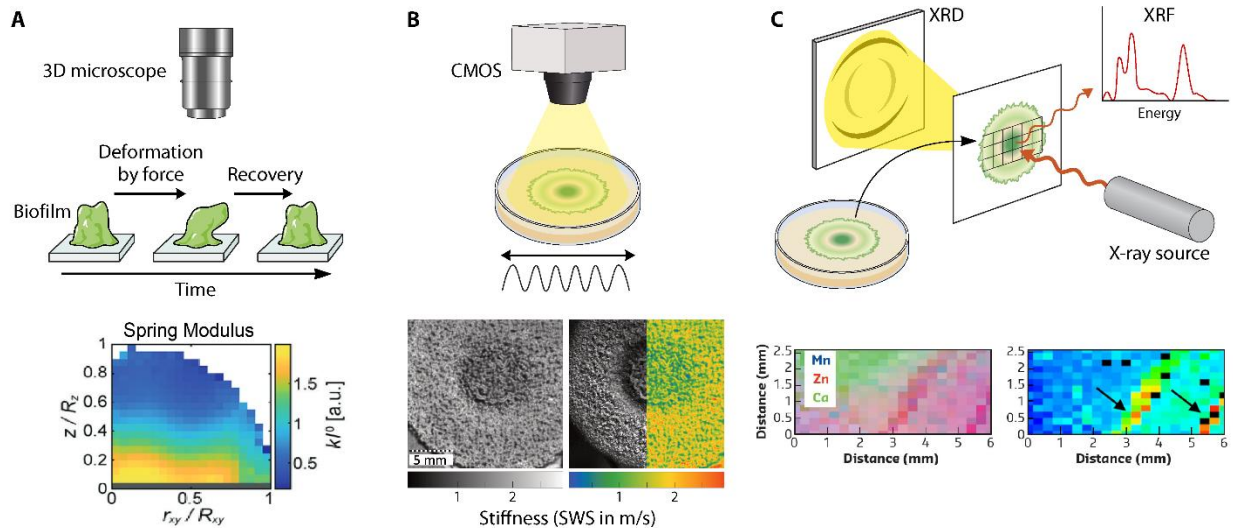
### 830 **6.2 Optical elastography**

831 Elastography, a technique used to quantify tissue and organ stiffness variations using  
832 ultrasound or magnetic resonance imaging, has emerged as a promising tool for biofilm  
833 research. *B. subtilis* colonies grown on agar were transferred with a piece of underlying  
834 agar (thus not perturbing the colony) onto a piezo actuator (**Figure 6B**). An actuator was  
835 vibrated horizontally with a short burst (~2 s) of frequencies in the kHz range. For thin-  
836 layer samples like biofilms growing on agar, shaking gives rise to shear waves  
837 propagating in the plane of vibrations in biofilms. For opaque biofilms, optical imaging is  
838 able to trace surface displacements due to horizontal shear waves. By using multi-

839 frequency inversion, a spatially resolved map of the elastic modulus (**Figure 6B**) could  
 840 be created. These measurements showed that the central part of the colony was softer  
 841 compared to its periphery, softening of the biofilm with its age, and changes of material  
 842 properties in the regions of biofilm wrinkles that cover water filled channels (187).  
 843 Importantly, the obtained absolute values of the storage modulus in the range of 1-4 kPa  
 844 were consistent with previously reported bulk measurements for biofilms (174). This  
 845 promising novel technique is the first to deliver non-invasive, highly spatially-resolved  
 846 mechanical characterization of whole living biofilm colonies with  $\mu\text{m}$  resolution. Since the  
 847 measurement just takes several seconds, it can be repeated almost as a time lapse  
 848 sequence following the development of the biofilm. The relatively inexpensive and simple  
 849 setup makes it accessible to any laboratory. It needs to be mentioned, though, that the  
 850 interpretation of results in complex architectures containing slip interfaces such as water-  
 851 filled channels under biofilm wrinkles is still open (178).

852  
 853 Extremely short and non-invasive measurements allow this technique to be combined  
 854 with any other tool in a sequential manner. It will be interesting to study how the biofilm  
 855 material properties change in response to mechanical perturbations (i.e. stretching,  
 856 bending, or local damage) and osmotic or biochemical stresses.

857  
 858



859  
 860

861 **Figure 6. Methods for mechanical and structural characterization of biofilms.** **A:** 3D  
 862 imaging of biofilms and tracking all individual cells during the deformation and recovery  
 863 of the biofilm upon a mechanical deformation (top) allows to computationally infer the  
 864 elastic modulus of the biofilm with spatial resolution (bottom) (176). **B:** Schematics of the  
 865 image-based elastography setup, where a biofilm sample is vibrated by a piezo-actuator  
 866 in horizontal direction (top). Displacements on the surface of the sample due to thus

867 generated shear waves are imaged by a fast camera. With the help of reconstruction  
868 algorithms shear wave speeds are calculated and linked to the material properties. An  
869 example of a biofilm elastography sample (bottom) with a zoom in into the central area of  
870 the biofilm. Wrinkles on the surface of the biofilm are also visible in the maps of the shear  
871 wave speeds (SWS). Image courtesy J. Jordan and I. Sack, for experimental details see  
872 (178). **C**: Schematics of the X-ray diffraction (XRD)/fluorescence (XRF) setup, with a  
873 biofilm sample irradiated with a synchrotron X-ray beam and XRD/XRF signals collected  
874 simultaneously (top). XRD signal map of a biofilm piece, showing increased spore signal  
875 along biofilm wrinkles (marked with arrows) (bottom right). XRF signal map of the same  
876 biofilm piece (at the bottom right), revealing metal ion accumulation (e.g. Mn and Zn but  
877 not Ca) at the biofilm wrinkles (bottom left). Images reproduced from (163) with  
878 permissions of authors. Schematics of setups are not drawn to scale.

### 879 **6.3 X-ray synchrotron diffraction and fluorescence**

880 X-ray radiation has been used in medicine to discriminate soft from hard tissues (e.g.,  
881 teeth and bone) and in scientific laboratories mostly to decipher the properties of organic  
882 crystals and inorganic minerals. Thanks to the atomic scale wavelength of X-rays,  
883 diffraction (X-ray diffraction, XRD) exposes periodic atomic structures, for example of  
884 teeth and bone (188, 189), whereas scattering (e.g. small angle X-ray scattering, SAXS)  
885 reveals dimension shape of larger scale and soft objects, such as brain tumors (190).  
886 Just like eukaryotic tissues, biofilms are soft materials and even structurally ordered  
887 molecules therein are often isotropic and therefore they are not expected to diffract. Yet,  
888 it was recently shown that mapping the X-ray scattering of whole biofilms may become  
889 handy in spatially resolving the distribution of macromolecules and water and even  
890 discriminating between the different states of water (163).

891 Synchrotron radiation facility beamlines provide brilliant X-ray beams allowing fast  
892 mapping with remarkable spatial resolution. The experimental conditions for biofilm  
893 measurements vary depending on the synchrotron facility and the specific beamline, and  
894 the acquisition time may vary between ms/point and tens of seconds/point, depending on  
895 the photon flux and the sample thickness. The choice of a synchrotron facility and tuning  
896 the measuring conditions are therefore important for the success of an experiment, and  
897 they should reflect the balance between scanning area and the measurement resolution  
898 (for XRD) and the absorption cross-section of the elements under study (for X-ray  
899 fluorescence, XRF). Above all, given that beam-induced radiation damage biofilms may  
900 extend beyond the dimensions of the beam size, especially for hydrated samples, correct  
901 experimental conditions are crucial to minimizing beam damage (**Figure 6C**).

902  
903 Combining XRD with XRF, as is now commonly feasible in synchrotron facilities (179,  
904 180), reveals complementary knowledge on the spatial distribution of periodic structures  
905 (XRD) and metals ions (XRF) in whole biofilms (see **Figure 6C** top panel for schematics

906 and bottom panel for results). Such a combined XRD/XRF study across whole biofilms  
907 suggested that enhanced water evaporation from the surface of longitudinal biofilm  
908 wrinkles (187) assists the accumulation of metal ions in biofilms but more so along the  
909 wrinkles. Interestingly, cells displaying characteristic diffraction patterns, in this case  
910 bacterial spores, are also mapped on the positions of the wrinkles. This suggests that the  
911 evaporation driven accumulation of metal ions in the wrinkles may be a driver of  
912 sporulation (see the mapping of metal ions XRF and spore XRD signals in **Figure 6C**  
913 bottom left and right panels respectively). Therefore, a combination of XRD/XRF enables  
914 the direct observation of sporulation processes without requiring genetic labeling  
915 techniques or specific markers (163) along with the distribution of water and essential  
916 metal ions.

917  
918 While XRD/XRF mapping provides structural information on spatial heterogeneities of  
919 molecular structure and metal ion composition, the possible coupling between metal ion  
920 distribution and genetic expression on a macroscopic length scale calls for a combination  
921 of additional methods. To obtain an even more complete picture of the biofilm as the result  
922 of coordinated gene expression and secreted small molecules, information from  
923 complementary methods such as MALDI-imaging and spatial mRNA sequencing – as  
924 described above – should be considered.

## 925 **Conclusions**

926  
927 The central focus of this review was to provide an overview of emerging cutting-edge  
928 technologies that are just beginning to conquer studies of bacterial populations. Although  
929 these technologies are still challenging to use, they are very useful for resolving  
930 macroscopic structures (mm range) down to micron resolution, i.e. at the level of  
931 individual microbial cells. Achieving this resolution within structured populations is only  
932 now becoming available or is still in development. But the key technologies are in place  
933 to study truly multicellular physiological traits that are the result of phenotypic  
934 heterogeneity and spatiotemporally controlled differentiation programs within structured  
935 and at least transiently stable microbial populations, giving rise to properties not observed  
936 at the single-cell level or in dispersed cultures. The current body of evidence already  
937 indicates that such emerging multicellular functions can only be detected and understood  
938 by combinations of the methods described in this review. Accordingly, research is only at  
939 the very beginning of gaining a mechanistic insight and molecular understanding of the  
940 multicellular nature of bacterial life in structured populations.

941  
942 This review highlights examples of the application of these techniques for resolving  
943 emergent functions in multicellular bacterial populations, with a special emphasis on  
944 bacterial colonies as a structured form of biofilms. From a physiological point of view, this

945 review focused exclusively on resolving the multicellular properties of bacterial colonies,  
946 i.e. a clonal form of spatiotemporally differentiated but isogenic biofilms, and their  
947 emergent functions.

948  
949 The exciting discoveries that are currently being made on the evolutionary questions  
950 surrounding the traits of multicellularity indicate that even for traditionally unicellular  
951 organisms, the multicellular population may be the unit for evolution and selection – at  
952 least for some multicellular functions. In this context, complexly structured biofilms and  
953 colonies can represent a multicellular organism without the individual cells having become  
954 terminally differentiated. Addressing this fundamental question promises to yield a wealth  
955 of novel insights, as anticipated from the studies outlined above.

956

### 957 **Acknowledgements**

958 This work was supported by the Deutsche Forschungsgemeinschaft (DFG) within the  
959 SPP 2389 priority program “Emergent Functions of Bacterial Multicellularity” (Grants  
960 SSEM, AES: 503267551; GA, SM: 503905203; WRH: 503940974; VZ, LC: 504222949; KD:  
961 504072468; KD, TM: 504017689, AG: 504072468; CW: 503995533).

962

963

### 964 **References**

965

- 966 1. Grosberg RK, Strathmann RR. 2007. The evolution of multicellularity: A minor major transition? *Annu*  
967 *Rev Ecol Evol Syst* 38:621–654.
- 968 2. Fisher RM, Cornwallis CK, West SA. 2013. Group formation, relatedness, and the evolution of  
969 multicellularity. *Curr Biol* 23:1120–1125.
- 970 3. Bingham EP, Ratcliff WC. 2024. A nonadaptive explanation for macroevolutionary patterns in the  
971 evolution of complex multicellularity. *Proc Natl Acad Sci* 121:e2319840121.
- 972 4. Lyons NA, Kolter R. 2015. On the evolution of bacterial multicellularity. *Curr Opin Microbiol* 24:21–28.
- 973 5. Oldewurtel ER, Kouzel N, Dewenter L, Henseler K, Maier B. 2015. Differential interaction forces  
974 govern bacterial sorting in early biofilms. *Elife* 4:1–21.
- 975 6. Arnaouteli S, Bamford NC, Stanley-Wall NR, Kovács ÁT. 2021. *Bacillus subtilis* biofilm formation and  
976 social interactions. *Nat Rev Microbiol* 19:600–614.
- 977 7. Bretl DJ, Kirby JR. 2016. Molecular mechanisms of signaling in *Myxococcus xanthus* development. *J*  
978 *Mol Biol* 428:3805–3830.
- 979 8. Zambri MP, Williams MA, Elliot MA. 2022. Zambri MP, Williams MA, Elliot MA. How *Streptomyces*  
980 thrive: Advancing our understanding of classical development and uncovering new behaviors. *Adv*  
981 *Microb Physiol* 80:203-236.
- 982 9. Zeng X, Zhang CC. 2022. The making of a heterocyst in Cyanobacteria. *Annu Rev Microbiol* 76:597–  
983 618.
- 984 10. Shapiro JA. 1998. Thinking about bacterial populations as multicellular organisms. *Annu Rev*  
985 *Microbiol* 52:81–104.
- 986 11. Shapiro JA. 1 June 1988. Bacteria as multicellular organisms. *Sci Am* 1988  
987 DOI:10.1038/scientificamerican0688-82
- 988 12. Veening JW, Smits WK, Kuipers OP. 2008. Bistability, epigenetics, and bet-hedging in bacteria. *Annu*  
989 *Rev Microbiol* 62:193–210.
- 990 13. Steenackers HP, Parijs I, Dubey A, Foster KR, Vanderleyden J. 2016. Experimental evolution in  
991 biofilm populations. *FEMS Microbiol Rev* 40:373–397.

- 992 14. Bich L, Pradeu T, Moreau JF. 2019. Understanding multicellularity: The functional organization of the  
993 intercellular space. *Front Physiol* 10:1170
- 994 15. Hengge R. 2020. Linking bacterial growth, survival, and multicellularity – small signaling molecules as  
995 triggers and drivers. *Curr Opin Microbiol* 55:57–66.
- 996 16. Jahn M, Vorpahl C, Türkowsky D, Lindmeyer M, Bühler B, Harms H, Müller S. 2014. Accurate  
997 determination of plasmid copy number of flow-sorted cells using droplet digital PCR. *Anal Chem*  
998 86:5969–5976.
- 999 17. Keegstra JM, Kamino K, Anquez F, Lazova MD, Emonet T, Shimizu TS. 2017. Phenotypic diversity  
1000 and temporal variability in a bacterial signaling network revealed by single-cell FRET. *Elife* 6:e27455.
- 1001 18. Manina G, Griego A, Singh LK, McKinney JD, Dhar N. 2019. Preexisting variation in DNA damage  
1002 response predicts the fate of single mycobacteria under stress. *EMBO J* 38:1–19.
- 1003 19. Flores E, Herrero A. 2010. Compartmentalized function through cell differentiation in filamentous  
1004 cyanobacteria. *Nat Rev Microbiol* 8:39–50.
- 1005 20. Ye Y, Ghrayeb M, Miercke S, Arif S, Müller S, Mascher T, Chai L, Zaburdaev V. 2023. Residual cells  
1006 and nutrient availability guide wound healing in bacterial biofilms. *Soft Matter* 20:1047–1060.
- 1007 21. Hartmann R, Singh PK, Pearce P, Mok R, Song B, Díaz-Pascual F, Dunkel J, Drescher K. 2019.  
1008 Emergence of three-dimensional order and structure in growing biofilms. *Nat Phys* 15:251–256.
- 1009 22. Zhang M, Zhang J, Wang Y, Wang J, Achimovich AM, Acton ST, Gahlmann A. 2020. Non-invasive  
1010 single-cell morphometry in living bacterial biofilms. *Nat Commun* 11:1–13.
- 1011 23. Yordanov S, Neuhaus K, Hartmann R, Díaz-Pascual F, Vidakovic L, Singh PK, Drescher K. 2021.  
1012 Single-objective high-resolution confocal light sheet fluorescence microscopy for standard biological  
1013 sample geometries. *Biomed Opt Express* 12:3372.
- 1014 24. Díaz-Pascual F, Lempp M, Noshok K, Jeckel H, Jo JK, Neuhaus K, Hartmann R, Jelli E, Hansen MF,  
1015 Price-Whelan A, Dietrich LE, Link H, Drescher K. 2021. Spatial alanine metabolism determines local  
1016 growth dynamics of *Escherichia coli* colonies. *Elife* 10:1–29.
- 1017 25. Yordanov S, Neuhaus K, Hartmann R, Díaz-Pascual F, Vidakovic L, Singh PK, Drescher K. 2021.  
1018 Single-objective high-resolution confocal light sheet fluorescence microscopy for standard biological  
1019 sample geometries. *Biomed Opt Express* 12:3372–3391.
- 1020 26. Heydorn A, Nielsen AT, Hentzer M, Sternberg C, Givskov M, Ersboll BK, Molin S. 2000.  
1021 Quantification of biofilm structures by the novel computer program COMSTAT. *Microbiology*  
1022 146:2395–2407.
- 1023 27. Vorregaard M. 2008. PhD thesis. Comstat2 - a modern 3D image analysis environment for biofilms.  
1024 Technical University of Denmark, Kongens Lyngby, Denmark
- 1025 28. Mueller LN, de Brouwer JFC, Almeida JS, Stal LJ, Xavier JB. 2006. Analysis of a marine phototrophic  
1026 biofilm by confocal laser scanning microscopy using the new image quantification software PHLIP.  
1027 *BMC Ecol* 6:1.
- 1028 29. Daims H, Lückner S, Wagner M. 2005. Daime, a novel image analysis program for microbial ecology  
1029 and biofilm research. *Environ Microbiol* 8:200–213.
- 1030 30. Hartmann R, Jeckel H, Jelli E, Singh PK, Vaidya S, Bayer M, Rode DKH, Vidakovic L, Díaz-Pascual  
1031 F, Fong JCN, Dragoš A, Lamprecht O, Thöming JG, Netter N, Häussler S, Nadell CD, Sourjik V,  
1032 Kovács ÁT, Yildiz FH, Drescher K. 2021. Quantitative image analysis of microbial communities with  
1033 BiofilmQ. *Nat Microbiol* 6:151–156.
- 1034 31. Hartmann R, van Teeseling MCF, Thanbichler M, Drescher K. 2020. BacStalk: A comprehensive and  
1035 interactive image analysis software tool for bacterial cell biology. *Mol Microbiol* 114:140–150.
- 1036 32. Paintdakhi A, Parry B, Campos M, Irnov I, Elf J, Surovtsev I, Jacobs-Wagner C. 2016. Oufiti: An  
1037 integrated software package for high-accuracy, high-throughput quantitative microscopy analysis. *Mol*  
1038 *Microbiol* 99:767–777.
- 1039 33. Ducret A, Quardokus EM, Brun Y V. 2016. MicrobeJ, a tool for high throughput bacterial cell detection  
1040 and quantitative analysis. *Nat Microbiol* 1:16077.
- 1041 34. Lugagne JB, Lin H, Dunlop MJ. 2020. Delta: Automated cell segmentation, tracking, and lineage  
1042 reconstruction using deep learning. *PLoS Comput Biol* 16:1–18.
- 1043 35. Stylianidou S, Brennan C, Nissen SB, Kuwada NJ, Wiggins PA. 2016. SuperSegger: robust image  
1044 segmentation, analysis and lineage tracking of bacterial cells. *Mol Microbiol* 102:690–700.
- 1045 36. Drescher K, Dunkel J, Nadell CD, Van Teeffelen S, Grnja I, Wingreen NS, Stone HA, Bassler BL.  
1046 2016. Architectural transitions in *Vibrio cholerae* biofilms at single-cell resolution. *Proc Natl Acad Sci*  
1047 U S A 113(14):E2066-72.

- 1048 37. Stewart EJ, Satorius AE, Younger JG, Solomon MJ. 2013. Role of environmental and antibiotic stress  
1049 on *Staphylococcus epidermidis* biofilm microstructure. *Langmuir* 29(23):7017-24.
- 1050 38. Jelli E, Ohmura T, Netter N, Abt M, Jiménez-Siebert E, Neuhaus K, Rode DKH, Nadell CD, Drescher  
1051 K. 2023. Single-cell segmentation in bacterial biofilms with an optimized deep learning method  
1052 enables tracking of cell lineages and measurements of growth rates. *Mol Microbiol* 119:659–676.
- 1053 39. Zhang J, Wang Y, Donarski ED, Toma TT, Miles MT, Acton ST, Gahlmann A. 2022. BCM3D 2.0:  
1054 accurate segmentation of single bacterial cells in dense biofilms using computationally generated  
1055 intermediate image representations. *NPJ Biofilms Microbiomes* 8(1):99
- 1056 40. Cui D, Kong L, Wang Y, Zhu Y, Zhang C. 2022. In situ identification of environmental microorganisms  
1057 with Raman spectroscopy. *Environ Sci Ecotechnology* 11:100187.
- 1058 41. Ciobotă V, Burkhardt E-M, Schumacher W, Rösch P, Küsel K, Popp J. 2010. The influence of  
1059 intracellular storage material on bacterial identification by means of Raman spectroscopy. *Anal*  
1060 *Bioanal Chem* 397:2929–2937.
- 1061 42. Wang Y, Song Y, Tao Y, Muhamadali H, Goodacre R, Zhou N-Y, Preston GM, Xu J, Huang WE.  
1062 2016. Reverse and multiple stable isotope probing to study bacterial metabolism and interactions at  
1063 the single cell level. *Anal Chem* 88:9443–9450.
- 1064 43. Wang Y, Xu J, Kong L, Liu T, Yi L, Wang H, Huang WE, Zheng C. 2020. Raman-deuterium isotope  
1065 probing to study metabolic activities of single bacterial cells in human intestinal microbiota. *Microb*  
1066 *Biotechnol* 13:572–583.
- 1067 44. Berry D, Mader E, Lee TK, Woebken D, Wang Y, Zhu D, Palatinszky M, Schintlmeister A, Schmid  
1068 MC, Hanson BT, Shterzer N, Mizrahi I, Rauch I, Decker T, Bocklitz T, Popp J, Gibson CM, Fowler  
1069 PW, Huang WE, Wagner M. 2015. Tracking heavy water (D2O) incorporation for identifying and  
1070 sorting active microbial cells. *Proc Natl Acad Sci* 112:E194–E203.
- 1071 45. Parmar D, Rosado-Rosa JM, ShROUT JD, Sweedler J V. 2024. Metabolic insights from mass  
1072 spectrometry imaging of biofilms: A perspective from model microorganisms. *Methods* 224:21–34.
- 1073 46. Couvillion SP, Zhu Y, Nagy G, Adkins JN, Ansong C, Renslow RS, Piehowski PD, Ibrahim YM, Kelly  
1074 RT, Metz TO. 2019. New mass spectrometry technologies contributing towards comprehensive and  
1075 high throughput omics analyses of single cells. *Analyst* 144:794–807.
- 1076 47. Hu H, Yin R, Brown HM, Laskin J. 2021. Spatial segmentation of mass spectrometry imaging data by  
1077 combining multivariate clustering and univariate thresholding. *Anal Chem* 93:3477–3485.
- 1078 48. Bien T, Koerfer K, Schwenzfeier J, Dreisewerd K, Soltwisch J. 2022. Mass spectrometry imaging to  
1079 explore molecular heterogeneity in cell culture. *Proc Natl Acad Sci U S A* 119:1–12.
- 1080 49. Niehaus M, Soltwisch J, Belov ME, Dreisewerd K. 2019. Transmission-mode MALDI-2 mass  
1081 spectrometry imaging of cells and tissues at subcellular resolution. *Nat Methods* 16:925–931.
- 1082 50. Soltwisch J, Kettling H, Vens-Cappell S, Wiegelmann M, Müthing J, Dreisewerd K. 2015. Mass  
1083 spectrometry imaging with laser-induced postionization. *Science* 348(6231):211-5.
- 1084 51. Brockmann EU, Steil D, Bauwens A, Soltwisch J, Dreisewerd K. 2019. Advanced methods for MALDI-  
1085 MS Imaging of the chemical communication in microbial communities. *Anal Chem* 91:15081–15089.
- 1086 52. Rivera ES, Weiss A, Migas LG, Freiberg JA, Djambazova K V., Neumann EK, Van de Plas R,  
1087 Spraggins JM, Skaar EP, Caprioli RM. 2022. Imaging mass spectrometry reveals complex lipid  
1088 distributions across *Staphylococcus aureus* biofilm layers. *J Mass Spectrom Adv Clin Lab* 26:36–46.
- 1089 53. Singhal N, Kumar M, Kanaujia PK, Virdi JS. 2015. MALDI-TOF mass spectrometry: an emerging  
1090 technology for microbial identification and diagnosis. *Front Microbiol* 6:791.
- 1091 54. Calderaro A, Chezzi C. 2024. MALDI-TOF MS: a reliable tool in the real life of the clinical  
1092 microbiology laboratory. *Microorganisms* 12(2):322.
- 1093 55. Höfler C, Heckmann J, Fritsch A, Popp P, Gebhard S, Fritz G, Mascher T. 2016. Cannibalism stress  
1094 response in *Bacillus subtilis*. *Microbiol (Reading)* 162(1):164-176.
- 1095 56. Si T, Li B, Zhang K, Xu Y, Zhao H, Sweedler J V. 2016. Characterization of *Bacillus subtilis* colony  
1096 biofilms via mass spectrometry and fluorescence imaging. *J Proteome Res* 15:1955–1962.
- 1097 57. Jeckel H, Noshok K, Neuhaus K, Hastewell AD, Skinner DJ, Saha D, Netter N, Paczia N, Dunkel J,  
1098 Drescher K. 2023. Simultaneous spatiotemporal transcriptomics and microscopy of *Bacillus subtilis*  
1099 swarm development reveal cooperation across generations. *Nat Microbiol* 8:2378–2391.
- 1100 58. Abbaszade G, Stückerath K, Müller S. 2024. Bacterial colony biopsies: spatial discrimination of  
1101 heterogeneous cell types by cytometric fingerprinting. *Methods Ecol Evol* (under review).

- 1102 59. Cichocki N, Hübschmann T, Schattenberg F, Kerckhof FM, Overmann J, Müller S. 2020. Bacterial  
1103 mock communities as standards for reproducible cytometric microbiome analysis. *Nat Protoc*  
1104 15:2788–2812.
- 1105 60. Rao NS, Lundberg L, Palmkron S, Håkansson S, Bergenståhl B, Carlquist M. 2021. Flow cytometric  
1106 analysis reveals culture condition dependent variations in phenotypic heterogeneity of  
1107 *Limosilactobacillus reuteri*. *Sci Rep* 11:1–12.
- 1108 61. Schulze K, López DA, Tillich UM, Frohme M. 2011. A simple viability analysis for unicellular  
1109 cyanobacteria using a new autofluorescence assay, automated microscopy, and ImageJ. *BMC*  
1110 *Biotechnol* 11:118.
- 1111 62. Lambrecht J, Cichocki N, Hübschmann T, Koch C, Harms H, Müller S. 2017. Flow cytometric  
1112 quantification, sorting and sequencing of methanogenic archaea based on F420 autofluorescence.  
1113 *Microb Cell Fact* 16:1–15.
- 1114 63. Harris RL, Vetter MCYL, van Heerden E, Cason E, Vermeulen JG, Taneja A, Kieft TL, DeCoste CJ,  
1115 Laevsky GS, Onstott TC. 2022. FISH-TAMB, a fixation-free mRNA fluorescent labeling technique to  
1116 target transcriptionally active members in microbial communities. *Microb Ecol* 84:182–197.
- 1117 64. Müller S, Nebe-Von-Caron G. 2010. Functional single-cell analyses: Flow cytometry and cell sorting  
1118 of microbial populations and communities. *FEMS Microbiol Rev* 34:554–587.
- 1119 65. Müller S. 2007. Modes of cytometric bacterial DNA pattern: a tool for pursuing growth. *Cell Prolif*  
1120 40:621–639.
- 1121 66. Keegstra JM, Kamino K, Anquez F, Lazova MD, Emonet T, Shimizu TS. 2017. Phenotypic diversity  
1122 and temporal variability in a bacterial signaling network revealed by single-cell FRET. *Elife* 6:e27455.
- 1123 67. Armbruster CR, Lee CK, Parker-Gilham J, De Anda J, Xia A, Zhao K, Murakami K, Tseng BS,  
1124 Hoffman LR, Jin F, Harwood CS, Wong GCL, Parsek MR. 2019. Heterogeneity in surface sensing  
1125 suggests a division of labor in *Pseudomonas aeruginosa* populations. *Elife* 8:1–29.
- 1126 68. Nguyen TM, Telek S, Zicler A, Martinez JA, Zacchetti B, Kopp J, Slouka C, Herwig C, Grünberger A,  
1127 Delvigne F. 2021. Reducing phenotypic instabilities of a microbial population during continuous  
1128 cultivation based on cell switching dynamics. *Biotechnol Bioeng* 118:3847–3859.
- 1129 69. Rubbens P, Props R, Kerckhof F-M, Boon N, Waegeman W. 2021. PhenoGMM: Gaussian mixture  
1130 modeling of cytometry data quantifies changes in microbial community structure. *mSphere*  
1131 6(1):e00530-20.
- 1132 70. Bruckmann C, Müller S, Höner zu Siederdisen C. 2022. Automatic, fast, hierarchical, and non-  
1133 overlapping gating of flow cytometric data with flowEMMI v2. *Comput Struct Biotechnol J* 20:6473–  
1134 6489.
- 1135 71. Koch C, Fetzer I, Harms H, Müller S. 2013. CHIC-an automated approach for the detection of  
1136 dynamic variations in complex microbial communities. *Cytom Part A* 83 A:561–567.
- 1137 72. Koch C, Günther S, Desta AF, Hübschmann T, Müller S. 2013. Cytometric fingerprinting for analyzing  
1138 microbial intracommunity structure variation and identifying subcommunity function. *Nat Protoc*  
1139 8:190–202.
- 1140 73. Günther S, Koch C, Hübschmann T, Röske I, Müller RA, Bley T, Harms H, Müller S. 2012. Correlation  
1141 of community dynamics and process parameters as a tool for the prediction of the stability of  
1142 wastewater treatment. *Environ Sci Technol* 46:84–92.
- 1143 74. Kupschus J, Janssen S, Hoek A, Kuska J, Rathjens J, Sonntag C, Ickstadt K, Budzinski L, Chang  
1144 HD, Rossi A, Esser C, Hochrath K. 2022. Rapid detection and online analysis of microbial changes  
1145 through flow cytometry. *Cytom Part A* 103:419–428.
- 1146 75. Jahn M, Seifert J, von Bergen M, Schmid A, Bühler B, Müller S. 2013. Subpopulation-proteomics in  
1147 prokaryotic populations. *Curr Opin Biotechnol* 24:79–87.
- 1148 76. Végvári Á, Zhang X, Zubarev RA. 2023. Toward single bacterium proteomics. *J Am Soc Mass*  
1149 *Spectrom* 34:2098–2106.
- 1150 77. Freiherr von Boeselager R, Pfeifer E, Frunzke J. 2018. Cytometry meets next-generation sequencing  
1151 – RNA-Seq of sorted subpopulations reveals regional replication and iron-triggered prophage  
1152 induction in *Corynebacterium glutamicum*. *Sci Rep* 8:1–13.
- 1153 78. Imdahl F, Saliba AE. 2020. Advances and challenges in single-cell RNA-seq of microbial  
1154 communities. *Curr Opin Microbiol* 57:102–110.
- 1155 79. Jehmlich N, Hübschmann T, Gesell Salazar M, Völker U, Benndorf D, Müller S, Von Bergen M,  
1156 Schmidt F. 2010. Advanced tool for characterization of microbial cultures by combining cytomics and  
1157 proteomics. *Appl Microbiol Biotechnol* 88:575–584.

- 1158 80. Huffman RG, Leduc A, Wichmann C, Di Gioia M, Borriello F, Specht H, Derks J, Khan S, Khoury L,  
1159 Emmott E, Petelski AA, Perlman DH, Cox J, Zanoni I, Slavov N. 2023. Prioritized mass spectrometry  
1160 increases the depth, sensitivity and data completeness of single-cell proteomics. *Nat Methods*  
1161 20:714–722.
- 1162 81. Teoh CP, Lavin P, Yusof NA, González-Aravena M, Najimudin N, Cheah YK, Wong CMVL. 2023.  
1163 Transcriptomics analysis provides insights into the heat adaptation strategies of an Antarctic  
1164 bacterium, *Cryobacterium* sp. SO1. *Polar Biol* 46:185–197.
- 1165 82. Wang H, Zhang Y, Bartlett DH, Xiao X. 2021. Transcriptomic analysis reveals common adaptation  
1166 mechanisms under different stresses for moderately piezophilic bacteria. *Microb Ecol* 81:617–629.
- 1167 83. McNulty R, Sritharan D, Pahng SH, Meisch JP, Liu S, Brennan MA, Saxer G, Hormoz S, Rosenthal  
1168 AZ. 2023. Probe-based bacterial single-cell RNA sequencing predicts toxin regulation. *Nat Microbiol*  
1169 8:934–945.
- 1170 84. Ma P, Amemiya HM, He LL, Gandhi SJ, Nicol R, Bhattacharyya RP, Smillie CS, Hung DT. 2023.  
1171 Bacterial droplet-based single-cell RNA-seq reveals antibiotic-associated heterogeneous cellular  
1172 states. *Cell* 186:877–891.e14.
- 1173 85. Sánchez-Romero MA, Casadesús J. 2018. Contribution of SPI-1 bistability to *Salmonella enterica*  
1174 cooperative virulence: insights from single cell analysis. *Sci Rep* 8:1–11.
- 1175 86. Beebe DJ, Mensing GA, Walker GM. 2002. Physics and applications of microfluidics in biology. *Annu*  
1176 *Rev Biomed Eng* 4:261–286.
- 1177 87. Tabeling P. 2023. 'Introduction', Introduction to microfluidics, 2nd edn, p 1–47 (Oxford, 2023; online  
1178 edn, Oxford Academic), Oxford University Press.
- 1179 88. McDonald JC, Duffy DC, Anderson JR, Chiu DT, Wu H, Schueller OJA, Whitesides GM. 2000.  
1180 Fabrication of microfluidic systems in poly(dimethylsiloxane). *Electrophoresis* 21:27–40.
- 1181 89. Qin D, Xia Y, Whitesides GM. 2010. Soft lithography for micro- and nanoscale patterning. *Nat Protoc*  
1182 5:491–502.
- 1183 90. Prabhakar P, Sen RK, Dwivedi N, Khan R, Solanki PR, Srivastava AK, Dhand C. 2021. 3D-Printed  
1184 microfluidics and potential biomedical applications. *Front Nanotechnol* 3:1–16.
- 1185 91. Juang YJ, Chiu YJ. 2022. Fabrication of polymer microfluidics: An overview. *Polymers (Basel)* 14:1–  
1186 18.
- 1187 92. Garmasukis R, Hackl C, Charvat A, Mayr SG, Abel B. 2023. Rapid prototyping of microfluidic chips  
1188 enabling controlled biotechnology applications in microspace. *Curr Opin Biotechnol* 81:102948.
- 1189 93. Pérez-Rodríguez S, García-Aznar JM, Gonzalo-Asensio J. 2022. Microfluidic devices for studying  
1190 bacterial taxis, drug testing and biofilm formation. *Microb Biotechnol* 15:395–414.
- 1191 94. Yuan L, Straub H, Shishaeva L, Ren Q. 2023. Microfluidics for biofilm studies. *Annu Rev Anal Chem*  
1192 16:139–159.
- 1193 95. Long Z, Nugent E, Javer A, Cicuta P, Sclavi B, Cosentino Lagomarsino M, Dorfman KD. 2013.  
1194 Microfluidic chemostat for measuring single cell dynamics in bacteria. *Lab Chip* 13:947–954.
- 1195 96. Asayesh F, Zarabadi MP, Aznavah NB, Greener J. 2018. Microfluidic flow confinement to avoid  
1196 chemotaxis-based upstream growth in a biofilm flow cell reactor. *Anal Methods* 10:4579–4587.
- 1197 97. Straub H, Eberl L, Zinn M, Rossi RM, Maniura-Weber K, Ren Q. 2020. A microfluidic platform for in  
1198 situ investigation of biofilm formation and its treatment under controlled conditions. *J*  
1199 *Nanobiotechnology* 18:1–12.
- 1200 98. Kim KP, Kim YG, Choi CH, Kim HE, Lee SH, Chang WS, Lee CS. 2010. *In situ* monitoring of  
1201 antibiotic susceptibility of bacterial biofilms in a microfluidic device. *Lab Chip* 10:3296–3299.
- 1202 99. Tang PC, Eriksson O, Sjögren J, Fatsis-Kavalopoulos N, Kreuger J, Andersson DI. 2022. A  
1203 microfluidic chip for studies of the dynamics of antibiotic resistance selection in bacterial biofilms.  
1204 *Front Cell Infect Microbiol* 12:1–14.
- 1205 100. Bae AJ, Beta C, Bodenschatz E. 2009. Rapid switching of chemical signals in microfluidic devices.  
1206 *Lab Chip* 9:3059–3065.
- 1207 101. Westerwalbesloh C, Grünberger A, Stute B, Weber S, Wiechert W, Kohlheyer D, Von Lieres E. 2015.  
1208 Modeling and CFD simulation of nutrient distribution in picoliter bioreactors for bacterial growth  
1209 studies on single-cell level. *Lab Chip* 15:4177–4186.
- 1210 102. Zoheir AE, Stolle C, Rabe KS. 2024. Microfluidics for adaptation of microorganisms to stress: design  
1211 and application. *Appl Microbiol Biotechnol* 108(1):162.
- 1212 103. Rochex A, Godon JJ, Bernet N, Escudié R. 2008. Role of shear stress on composition, diversity and  
1213 dynamics of biofilm bacterial communities. *Water Res* 42:4915–4922.

- 1214 104. Wilking JN, Angelini TE, Seminara A, Brenner MP, Weitz DA. 2011. Biofilms as complex fluids. *MRS*  
1215 *Bull* 36:385–391.
- 1216 105. Tsagakari E, Connelly S, Liu Z, McBride A, Sloan WT. 2022. The role of shear dynamics in biofilm  
1217 formation. *NPJ Biofilms Microbiomes* 8(1):33.
- 1218 106. Park A, Jeong HH, Lee J, Kim KP, Lee CS. 2011. Effect of shear stress on the formation of bacterial  
1219 biofilm in a microfluidic channel. *Biochip J* 5:236–241.
- 1220 107. Lambert G, Kussel E. 2014. Memory and fitness optimization of bacteria under fluctuating  
1221 environments. *PLoS Genet* 10(9):e1004556
- 1222 108. Nguyen J, Fernandez V, Pontrelli S, Sauer U, Ackermann M, Stocker R. 2021. A distinct growth  
1223 physiology enhances bacterial growth under rapid nutrient fluctuations. *Nat Commun* 12:3662.
- 1224 109. Kaiser M, Jug F, Julou T, Deshpande S, Pfohl T, Silander OK, Myers G, van Nimwegen E. 2018.  
1225 Monitoring single-cell gene regulation under dynamically controllable conditions with integrated  
1226 microfluidics and software. *Nat Commun* 9:212.
- 1227 110. Fenchel T. 2002. Microbial behavior in a heterogeneous world. *Science* 296(5570):1068-71.
- 1228 111. Donaldson GP, Lee SM, Mazmanian SK. 2016. Gut biogeography of the bacterial microbiota. *Nat*  
1229 *Rev Microbiol* 14:20–32.
- 1230 112. Motta JP, Wallace JL, Buret AG, Deraison C, Vergnolle N. 2021. Gastrointestinal biofilms in health  
1231 and disease. *Nat Rev Gastroenterol Hepatol* 18:314–334.
- 1232 113. Karita Y, Limmer DT, Hallatschek O. 2022. Scale-dependent tipping points of bacterial colonization  
1233 resistance. *Proc Natl Acad Sci U S A* 119:1–7.
- 1234 114. Postek W, Staśkiewicz K, Lilja E, Waclaw B. 2024. Substrate geometry affects population dynamics  
1235 in a bacterial biofilm. *Proc Natl Acad Sci* 121:e2315361121.
- 1236 115. Kurz DL, Secchi E, Carrillo FJ, Bourg IC, Stocker R, Jimenez-Martinez J. 2022. Competition between  
1237 growth and shear stress drives intermittency in preferential flow paths in porous medium biofilms.  
1238 *Proc Natl Acad Sci U S A* 119:1–10.
- 1239 116. Zoheir AE, Meisch L, Martín MV, Bickmann C, Kiselev A, Lenk F, Kaster AK, Rabe KS, Niemeyer  
1240 CM. 2022. Macroporous silicone chips for decoding microbial dark matter in environmental  
1241 microbiomes. *ACS Appl Mater Interfaces* 14(44):49592–603.
- 1242 117. Scheidweiler D, Bordoloi AD, Jiao W, Sentchilo V, Bollani M, Chhun A, Engel P, de Anna P. 2024.  
1243 Spatial structure, chemotaxis and quorum sensing shape bacterial biomass accumulation in complex  
1244 porous media. *Nat Commun* 15:1–12.
- 1245 118. Grünberger A, Probst C, Helfrich S, Nanda A, Stute B, Wiechert W, von Lieres E, Nöh K, Frunzke J,  
1246 Kohlheyer D. 2015. Spatiotemporal microbial single-cell analysis using a high-throughput  
1247 microfluidics cultivation platform. *Cytom Part A* 87:1101–1115.
- 1248 119. Scheidweiler D, Miele F, Peter H, Battin TJ, De Anna P. 2020. Trait-specific dispersal of bacteria in  
1249 heterogeneous porous environments: From pore to porous medium scale. *J R Soc Interface*  
1250 17(164):20200046.
- 1251 120. Nadell CD, Xavier JB, Foster KR. 2008. The sociobiology of biofilms. *FEMS Microbiol Rev* 33:206–  
1252 224.
- 1253 121. Hallatschek O, Nelson DR. 2010. Life at the front of an expanding population. *Evolution* 64(1):193-  
1254 206.
- 1255 122. Kayser J, Schreck CF, Yu Q, Gralka M, Hallatschek O. 2018. Emergence of evolutionary driving  
1256 forces in pattern-forming microbial populations. *Philos Trans R Soc Lond B Biol Sci*  
1257 373(1747):20170106.
- 1258 123. Ma T, Rothschild J, Halabeya F, Zilman A, Milstein JN. 2024. Mechanics limits ecological diversity  
1259 and promotes heterogeneity in confined bacterial communities. *Proc Natl Acad Sci U S A* 121:1–11.
- 1260 124. Hennes M, Bender N, Cronenberg T, Welker A, Maier B. 2023. Collective polarization dynamics in  
1261 bacterial colonies signify the occurrence of distinct subpopulations. *PLoS Biol* 21:1–20.
- 1262 125. Wang P, Robert L, Pelletier J, Dang WL, Taddei F, Wright A, Jun S. 2010. Robust growth of  
1263 *Escherichia coli*. *Curr Biol* 20:1099–1103.
- 1264 126. Grünberger A, Wiechert W, Kohlheyer D. 2014. Single-cell microfluidics: Opportunity for bioprocess  
1265 development. *Curr Opin Biotechnol* 29:15–23.
- 1266 127. Kampf J, Gerwig J, Kruse K, Cleverley R, Dormeyer M, Grünberger A, Kohlheyer D, Commichau FM,  
1267 Lewis RJ, Stülke J. 2018. Selective pressure for biofilm formation in *Bacillus subtilis*: Differential effect  
1268 of mutations in the master regulator *sinR* on bistability. *mBio* 9(5):e01464-18.

- 1269 128. Hansen SH, Kabbeck T, Radtke CP, Krause S, Krolitzki E, Peschke T, Gasmi J, Rabe KS, Wagner  
1270 M, Horn H, Hubbuch J, Gescher J, Niemeyer CM. 2019. Machine-assisted cultivation and analysis of  
1271 biofilms. *Sci Rep* 9:8933.
- 1272 129. Klein E, Weiler J, Wagner M, Čelikić M, Niemeyer CM, Horn H, Gescher J. 2022. Enrichment of  
1273 phosphate-accumulating organisms (PAOs) in a microfluidic model biofilm system by mimicking a  
1274 typical aerobic granular sludge feast/famine regime. *Appl Microbiol Biotechnol* 106:1313–1324.
- 1275 130. Drescher K, Shen Y, Bassler BL, Stone HA. 2013. Biofilm streamers cause catastrophic disruption of  
1276 flow with consequences for environmental and medical systems. *Proc Natl Acad Sci U S A* 110:4345–  
1277 4350.
- 1278 131. Ackermann M. 2015. A functional perspective on phenotypic heterogeneity in microorganisms. *Nat*  
1279 *Rev Microbiol* 13:497–508.
- 1280 132. Berlanga M, Guerrero R. 2016. Living together in biofilms: The microbial cell factory and its  
1281 biotechnological implications. *Microb Cell Fact* 15:1–11.
- 1282 133. Westermann AJ, Vogel J. 2021. Cross-species RNA-seq for deciphering host–microbe interactions.  
1283 *Nat Rev Genet* 22:361–378.
- 1284 134. Jovic D, Liang X, Zeng H, Lin L, Xu F, Luo Y. 2022. Single-cell RNA sequencing technologies and  
1285 applications: A brief overview. *Clin Transl Med* 12(3):e694.
- 1286 135. Jenniches L, Michaux C, Popella L, Reichardt S, Vogel J, Westermann AJ, Barquist L. 2024.  
1287 Improved RNA stability estimation through Bayesian modeling reveals most *Salmonella* transcripts  
1288 have subminute half-lives. *Proc Natl Acad Sci U S A* 121:1–28.
- 1289 136. Steglich C, Lindell D, Futschik M, Rector T, Steen R, Chisholm SW. 2010. Short RNA half-lives in the  
1290 slow-growing marine cyanobacterium *Prochlorococcus*. *Genome Biol* 11(5):R54.
- 1291 137. Dar D, Sorek R. 2018. Extensive reshaping of bacterial operons by programmed mRNA decay. *PLoS*  
1292 *Genet* 14:1–19.
- 1293 138. Zocher S, McCloskey A, Karasinsky A, Schulte R, Friedrich U, Lesche M, Rund N, Gage FH, Hetzer  
1294 MW, Toda T. 2024. Lifelong persistence of nuclear RNAs in the mouse brain. *Science* 384(6691):53-  
1295 59.
- 1296 139. Homberger C, Barquist L, Vogel J. 2022. Ushering in a new era of single-cell transcriptomics in  
1297 bacteria. *MicroLife* 3:1–9.
- 1298 140. Mariscal V, Herrero A, Flores E. 2007. Continuous periplasm in a filamentous, heterocyst-forming  
1299 cyanobacterium. *Mol Microbiol* 65:1139–1145.
- 1300 141. Weiss GL, Kieninger A-K, Maldener I, Forchhammer K, Pilhofer M. 2019. Structure and function of a  
1301 bacterial gap junction analog. *Cell* 178:374-384.e15.
- 1302 142. Ermakova M, Allahverdiyeva Y. 2015. Isolation of heterocysts from *Anabaena* sp. PCC 7120. *Bio-*  
1303 *protocol* 5:e1456.
- 1304 143. Haselkorn R. 1978. Heterocysts. *Annu Rev Plant Biol* 29:319–344.
- 1305 144. Park J-J, Lechno-Yossef S, Wolk CP, Vieille C. 2013. Cell-specific gene expression in *Anabaena*  
1306 *variabilis* grown phototrophically, mixotrophically, and heterotrophically. *BMC Genomics* 14:759.
- 1307 145. Zhao A, Sun J, Liu Y. 2023. Understanding bacterial biofilms: From definition to treatment strategies.  
1308 *Front Cell Infect Microbiol* 13:1–23.
- 1309 146. Jo J, Price-Whelan A, Dietrich LEP. 2022. Gradients and consequences of heterogeneity in biofilms.  
1310 *Nat Rev Microbiol* 20(10):593-607.
- 1311 147. Sauer K, Stoodley P, Goeres DM, Hall-Stoodley L, Burmølle M, Stewart PS, Bjarnsholt T. 2022. The  
1312 biofilm life cycle: expanding the conceptual model of biofilm formation. *Nat Rev Microbiol* 20:608–620.
- 1313 148. Rosenberg AB, Roco CM, Muscat RA, Kuchina A, Sample P, Yao Z, Graybuck LT, Peeler DJ,  
1314 Mukherjee S, Chen W, Pun SH, Sellers DL, Tasic B, Seelig G. 2018. Single-cell profiling of the  
1315 developing mouse brain and spinal cord with split-pool barcoding. *Science* 360:176–182.
- 1316 149. Blattman SB, Jiang W, Oikonomou P, Tavazoie S. 2020. Prokaryotic single-cell RNA sequencing by  
1317 in situ combinatorial indexing. *Nat Microbiol* 5:1192–1201.
- 1318 150. Kuchina A, Brettner LM, Paleologu L, Roco CM, Rosenberg AB, Carignano A, Kibler R, Hirano M,  
1319 DePaolo RW, Seelig G. 2021. Microbial single-cell RNA sequencing by split-pool barcoding. *Science*  
1320 371(6531):eaba5257.
- 1321 151. Pu Y, Yan X, Liao H, Wang C, Huang C, Zhang W, Guo C. 2024. An advanced bacterial single-cell  
1322 RNA-seq reveals biofilm heterogeneity. *eLife*13:RP97543

- 1323 152. Pountain AW, Jiang P, Yao T, Homae E, Guan Y, McDonald KJC, Podkowik M, Shopsin B, Torres  
1324 VJ, Golding I, Yanai I. 2024. Transcription–replication interactions reveal bacterial genome regulation.  
1325 Nature 626:661–669.
- 1326 153. Sheng K, Cao W, Niu Y, Deng Q, Zong C. 2017. Effective detection of variation in single-cell  
1327 transcriptomes using MATQ-seq. Nat Methods 14:267–270.
- 1328 154. Imdahl F, Vafadarnejad E, Homberger C, Saliba AE, Vogel J. 2020. Single-cell RNA-sequencing  
1329 reports growth-condition-specific global transcriptomes of individual bacteria. Nat Microbiol 5:1202–  
1330 1206.
- 1331 155. Homberger C, Hayward RJ, Barquist L. 2023. Improved bacterial single-cell RNA-seq through  
1332 automated MATQ-seq and Cas9-based removal of rRNA reads. mBio 14(2):e0355722.
- 1333 156. Wang B, Lin AE, Yuan J, Novak KE, Koch MD, Wingreen NS, Adamson B, Gitai Z. 2023. Single-cell  
1334 massively-parallel multiplexed microbial sequencing (M3-seq) identifies rare bacterial populations and  
1335 profiles phage infection. Nat Microbiol 8:1846–1862.
- 1336 157. Dar D, Dar N, Cai L, Newman DK. 2021. Spatial transcriptomics of planktonic and sessile bacterial  
1337 populations at single-cell resolution. Science 373(6556):eabi4882.
- 1338 158. Lignell A, Kerosuo L, Streichan SJ, Cai L, Bronner ME. 2017. Identification of a neural crest stem cell  
1339 niche by Spatial Genomic Analysis. Nat Commun 8:1830.
- 1340 159. Seminara A, Angelini TE, Wilking JN, Vlamakis H, Ebrahim S, Kolter R, Weitz DA, Brenner MP. 2012.  
1341 Osmotic spreading of *Bacillus subtilis* biofilms driven by an extracellular matrix. Proc Natl Acad Sci U  
1342 S A 109:1116–1121.
- 1343 160. Yan J, Fei C, Mao S, Moreau A, Wingreen NS, Košmrlj A, Stone HA, Bassler BL. 2019. Mechanical  
1344 instability and interfacial energy drive biofilm morphogenesis. eLife 8:e43920.
- 1345 161. Pönisch W, Eckenrode KB, Alzurqa K, Nasrollahi H, Weber C, Zaburdaev V, Biais N. 2018. Pili  
1346 mediated intercellular forces shape heterogeneous bacterial microcolonies prior to multicellular  
1347 differentiation. Sci Rep 8:1–10.
- 1348 162. Ido N, Lybman A, Hayet S, Azulay DN, Ghrayeb M, Liddawieh S, Chai L. 2020. *Bacillus subtilis*  
1349 biofilms characterized as hydrogels. Insights on water uptake and water binding in biofilms. Soft  
1350 Matter 16(26):6180-6190.
- 1351 163. Azulay DN, Spaeker O, Ghrayeb M, Wilsch-Bräuninger M, Scoppola E, Burghammer M, Zizak I,  
1352 Bertinetti L, Politi Y, Chai L. 2021. Multiscale X-ray study of *Bacillus subtilis* biofilms reveals  
1353 interlinked structural hierarchy and elemental heterogeneity. Proc Natl Acad Sci 119:e2118107119.
- 1354 164. Goodwin K, Nelson CM. 2021. Mechanics of Development. Dev Cell 56:240–250.
- 1355 165. Claessen D, Rozen DE, Kuipers OP, Søgaard-Andersen L, Van Wezel GP. 2014. Bacterial solutions  
1356 to multicellularity: A tale of biofilms, filaments and fruiting bodies. Nat Rev Microbiol 12:115–124.
- 1357 166. Watnick P, Kolter R. 2000. Biofilm, city of microbes. J Bacteriol 182:2675–2679.
- 1358 167. Gloag ES, Fabbri S, Wozniak DJ, Stoodley P. 2020. Biofilm mechanics: Implications in infection and  
1359 survival. Biofilm 2:100017.
- 1360 168. Flemming HC, van Hullebusch ED, Neu TR, Nielsen PH, Seviour T, Stoodley P, Wingender J, Wuertz  
1361 S. 2023. The biofilm matrix: multitasking in a shared space. Nat Rev Microbiol 21:70–86.
- 1362 169. Fong JCN, Rogers A, Michael AK, Parsley NC, Cornell WC, Lin YC, Singh PK, Hartmann R, Drescher  
1363 K, Vinogradov E, Dietrich LEP, Partch CL, Yildiz FH. 2017. Structural dynamics of RbmA governs  
1364 plasticity of *Vibrio cholerae* biofilms. eLife 6:e26163.
- 1365 170. Hou J, Wang C, Rozenbaum RT, Gusnaniar N, de Jong ED, Woudstra W, Geertsema-Doornbusch  
1366 GI, Ateman-Smit J, Sjollem J, Ren Y, Busscher HJ, van der Mei HC. 2019. Bacterial density and  
1367 biofilm structure determined by optical coherence tomography. Sci Rep 9:9794.
- 1368 171. Charlton SGV, White MA, Jana S, Eland LE, Jayathilake PG, Burgess JG, Chen J, Wipat A, Curtis  
1369 TP. 2019. Regulating, measuring, and modeling the viscoelasticity of bacterial biofilms. J Bacteriol  
1370 201(18):e00101-19.
- 1371 172. Guélon T, Mathias JD, Stoodley P. 2011. Advances in biofilm mechanics. In: Flemming HC,  
1372 Wingender J, Szewzyk U. (eds) Biofilm Highlights. Springer Series on Biofilms, vol 5. Springer, Berlin,  
1373 Heidelberg.
- 1374 173. Geisel S, Secchi E, Vermant J. 2022. Experimental challenges in determining the rheological  
1375 properties of bacterial biofilms. Interface Focus 12(6):20220032.
- 1376 174. Jana S, Charlton SG V, Eland LE, Burgess JG, Wipat A, Curtis TP, Chen J. 2020. Nonlinear  
1377 rheological characteristics of single species bacterial biofilms. NPJ Biofilms Microbiomes 6(1):19.

- 1378 175. Kesel S, Grumbein S, Gümperlein I, Tallawi M, Marel AK, Lieleg O, Opitz M. 2016. Direct comparison  
1379 of physical properties of *Bacillus subtilis* NCIB 3610 and B-1 biofilms. *Appl Environ Microbiol*  
1380 82:2424–2432.
- 1381 176. Ohmura T, Skinner DJ, Neuhaus K, Choi GPT, Dunkel J, Drescher K. 2024. *In Vivo* microrheology  
1382 reveals local elastic and plastic responses inside 3D bacterial biofilms. *Adv Mater* 36(29):e2314059.
- 1383 177. Kennedy BF, Wijesinghe P, Sampson DD. 2017. The emergence of optical elastography in  
1384 biomedicine. *Nat Photonics* 11:215–221.
- 1385 178. Jordan J, Jaitner N, Meyer T, Brahmè L, Ghrayeb M, Köppke J, Chandia SK, Zaburdaev V, Chai L,  
1386 Tzschätzsch H, Mura J, Hagemann AIH, Braun J, Sack I. 2023. Optical time-harmonic elastography  
1387 for multiscale stiffness mapping across the phylogenetic tree. *arXiv*  
1388 <https://doi.org/10.48550/arXiv.2312.07380>.
- 1389 179. Cotte M, Gonzalez V, Vanmeert F, Monico L, Dejoie C, Burghammer M, Huder L, de Nolf W, Fisher  
1390 S, Fazlic I, Chauffeton C, Wallez G, Jiménez N, Albert-Tortosa F, Salvadó N, Possenti E, Colombo C,  
1391 Ghirardello M, Comelli D, Clerici EA, Vivani R, Romani A, Costantino C, Janssens K, Taniguchi Y,  
1392 McCarthy J, Reichert H, Susini J. 2022. The “Historical Materials BAG”: a new facilitated access to  
1393 synchrotron x-ray diffraction analyses for cultural heritage materials at the European Synchrotron  
1394 Radiation Facility. *Molecules* 27:6.
- 1395 180. Riekel C, Burghammer M, Davies R. 2010. Progress in micro- and nano-diffraction at the ESRF ID13  
1396 beamline. *IOP Conf Ser Mater Sci Eng* 14:012013.
- 1397 181. Birjiniuk A, Billings N, Nance E, Hanes J, Ribbeck K, Doyle PS. 2014. Single particle tracking reveals  
1398 spatial and dynamic organization of the *Escherichia coli* biofilm matrix. *New J Phys* 16:1–13.
- 1399 182. Chew SC, Kundukad B, Seviour T, Van der Maarel JRC, Yang L, Rice SA, Doyle P, Kjelleberg S.  
1400 2014. Dynamic remodeling of microbial biofilms by functionally distinct exopolysaccharides. *MBio*  
1401 5:1–11.
- 1402 183. Rahman MU, Fleming DF, Wang L, Rumbaugh KP, Gordon VD, Christopher GF. 2022. Microrheology  
1403 of *Pseudomonas aeruginosa* biofilms grown in wound beds. *NPJ Biofilms Microbiomes* 8:1–9.
- 1404 184. Galy O, Latour-Lambert P, Zrelli K, Ghigo JM, Beloin C, Henry N. 2012. Mapping of bacterial biofilm  
1405 local mechanics by magnetic microparticle actuation. *Biophys J* 103:1400–1408.
- 1406 185. Zrelli K, Galy O, Latour-Lambert P, Kirwan L, Ghigo JM, Beloin C, Henry N. 2013. Bacterial biofilm  
1407 mechanical properties persist upon antibiotic treatment and survive cell death. *New J Phys* 15:1–17.
- 1408 186. Hart JW, Waigh TA, Lu JR, Roberts IS. 2019. Microrheology and spatial heterogeneity of  
1409 *Staphylococcus aureus* biofilms modulated by hydrodynamic shear and biofilm-degrading enzymes.  
1410 *Langmuir* 35:3553–3561.
- 1411 187. Wilking JN, Zaburdaev V, De Volder M, Losick R, Brenner MP, Weitz DA. 2012. Liquid transport  
1412 facilitated by channels in *Bacillus subtilis* biofilms. *Proc Natl Acad Sci U S A* 110:848–852.
- 1413 188. Lowenstam HA. 1981. Minerals formed by organisms. *Science* 211(4487):1126-31.
- 1414 189. Addadi L, Weiner S. 2014. Biomineralization: Mineral formation by organisms. *Phys Scr* 89: 098003.
- 1415 190. Eggebrecht AT, Ferradal SL, Robichaux-Viehoever A, Hassanpour MS, Dehghani H, Snyder AZ,  
1416 Hershey T, Culver JP. 2014. Mapping distributed brain function and networks with diffuse optical  
1417 tomography. *Nat Photonics* 8:448–454.
- 1418 191. López-Gálvez J, Schiessl K, Besmer MD, Bruckmann C, Harms H, Müller S. 2023. Development of  
1419 an automated online flow cytometry method to quantify cell density and fingerprint bacterial  
1420 communities. *Cells* 12(12):1559.

1421

1422

1423

## 1424 **Supplementary Information**

1425

1426 **SI MOVIE 1.** Cultivation of *Priestia megaterium* DSM 90 in batch culture on DSM 1  
1427 medium at room temperature for 28.5 h. Samples were harvested and fixated using a  
1428 standard formaldehyde/ethanol procedure (see standardized methods in: (59)), and  
1429 subsequently, the cellular DNA was stained with 0.24  $\mu\text{M}$  DAPI (191) and cells analyzed

1430 using the BD Influx v7 Cell Sorter (Becton, Dickinson and Company, Franklin Lakes, NJ,  
1431 USA). The blue 488 nm Sapphire OPS laser (400 mW) was applied for forward scattering  
1432 (FSC) and a 355 nm Genesis OPS laser (100 mW) was applied for DAPI excitation. The  
1433 pictures were taken by using AxioScope A1 fluorescence microscope, equipped with a  
1434 Zeiss AxioCam MRm camera (Carl Zeiss Jena, Germany). Left above: Movie based on  
1435 samples taken from the growth curve and measured by flow cytometry as DAPI vs. FSC  
1436 2D plots. 200,000 cells per sample were measured. Each point represents one cell. The  
1437 color highlights the increasing number of cells in the virtual z-axis, with the red color  
1438 indicating the highest number of cells per bin. The movie shows the typical phenotypic  
1439 distributions during logarithmic growth, which changes rapidly. Different cell types  
1440 developed, including vegetative cells (veg\_1n – veg\_4n), which are cells with duplicate  
1441 chromosome copies. The ‘replicating cells’ are those that are most dominant in the log  
1442 phase of growth and contain multiple copies of finished and unfinished replicated  
1443 chromosomes, please see also (65). The strain produced different types of spores (sp\_1  
1444 – sp\_6). Some of the cells were less stained with DAPI for unknown reasons, but differed  
1445 in scattering and intensity of the dye fluorescence: unknown cells uc\_1 – uc\_4. Right  
1446 above: growth curve, measured by OD over time. The moving orange dot highlights the  
1447 sampling and is directly connected to the 2D-plots appearing on the left. Left below: a  
1448 gate template was created according to the subpopulations that develop during growth.  
1449 These subpopulations provide information about changes in the number of cells per gate  
1450 over time and also enable sorting decisions to be made using FACS. In this case, several  
1451 gates were sorted and subjected to microscopy. Right below: Phase contrast images of  
1452 sorted cells from gates that are replicating: veg\_1, veg\_2, ‘replicating cells’; and from  
1453 gates in which spores have formed: sp\_1 – sp\_6.

1454  
1455  
1456  
1457  
1458  
1459  
1460  
1461  
1462  
1463  
1464  
1465  
1466  
1467  
1468  
1469

1470 **Author Bios:**

1471 **Suyen Solange Espinoza Miranda** is a postdoctoral scientist at the University of  
1472 Würzburg. She studied Biochemistry at John Brown University followed by working for  
1473 five years as a research scientist in Nicaragua. Suyen completed her PhD in Biology with  
1474 focus in Infectious diseases from Boston College (USA) in 2023 where she specialized in  
1475 the study of pneumococcal biofilms. Since 2023, she has been designing and optimizing  
1476 single-cell RNA sequencing protocols in bacteria.

1477 **Gorkhmaz Abbaszade** is a postdoctoral researcher at the Helmholtz Centre for  
1478 Environmental Research – UFZ in Leipzig, Germany. He pursued his studies in Ecology  
1479 and Soil Sciences while simultaneously working as a junior researcher in the  
1480 Radiobiology Department at the Azerbaijan National Academy of Sciences. Following the  
1481 completion of his Ph.D. in Environmental Microbiology from Eötvös Loránd University in  
1482 Hungary, he continued his research in bioremediation, focusing on the restoration of soils  
1483 contaminated with toxic elements as a postdoctoral fellow. Since 2023, he has been a  
1484 member of the Flow Cytometry Group at the Helmholtz Centre, where his research  
1485 focused on microbial population heterogeneity and single-cell analysis.

1486 **Wolfgang R. Hess** is professor of Genetics and Experimental Bioinformatics at the  
1487 University of Freiburg, Germany. He graduated from the Humboldt University in Berlin,  
1488 Germany, and was a postdoctoral fellow or visiting guest scientist at the Friedrich  
1489 Miescher Institute in Basel, Switzerland, at the CNRS in Roscoff, France, and at the MIT  
1490 in Boston, U.S. He was the funding director of the Ocean Genome Legacy Foundation  
1491 affiliated with New England Biolabs in Beverly, U.S. His laboratory focuses on the  
1492 molecular biology of cyanobacteria and other photosynthetic organisms and their  
1493 functions in the environment and in biotechnology. Current research activities are  
1494 centered on the analysis of regulatory RNAs and RNA binding proteins, small protein  
1495 functions, epigenetic modifications and cell differentiation processes in bacteria.

1496 **Knut Drescher** is Associate Professor of Biophysics and Microbiology at the Biozentrum  
1497 of the University of Basel. He studied physics at the University of Oxford, before  
1498 completing a PhD in biophysics at the University of Cambridge in 2011. He became  
1499 interested in microbiology and bacterial biofilms during his postdoc at Princeton University  
1500 from 2011-2014. In 2014, Knut Drescher started his own lab as a Max Planck Research  
1501 Group Leader at the Max Planck Institute for Terrestrial Microbiology in Marburg, where  
1502 he focused on combining methods from physics and molecular biology to understand the  
1503 development and function of bacterial biofilms. In 2015, Knut Drescher also became a  
1504 professor in the physics department at the University of Marburg. In 2021, his lab moved  
1505 to the Biozentrum at the University of Basel, and continues to combine methods from  
1506 physics and molecular biology to study bacterial biofilms.

1507 **Antoine-Emmanuel Saliba** is an Associate Professor at the University of Würzburg and  
1508 a group leader at the Helmholtz Institute for RNA-based Infection Research (HIRI). He  
1509 studied biochemical engineering at INSA Toulouse and earned his PhD at the Institut  
1510 Curie, where he developed microfluidic systems for analyzing rare cancer cells at the  
1511 single-cell level. After a postdoctoral fellowship at the European Molecular Biology

1512 Laboratory (EMBL) in Heidelberg, where he worked on protein-lipid interactions, he joined  
1513 Jörg Vogel's lab in Würzburg. There, he pioneered single-cell RNA sequencing to study  
1514 *Salmonella enterica* infections. Since 2017, he has led the Single-Cell Analysis group at  
1515 HIRI, advancing technologies to study host-pathogen interactions. In 2023, he was  
1516 appointed to a W2 professorship at the University of Würzburg's Faculty of Medicine.

1517 **Vasily Zaburdaev** is a professor of "Mathematics in Life Sciences" at the Friedrich-  
1518 Alexander-Universität Erlangen-Nürnberg. He received his PhD in Physics in 2004 at the  
1519 Russian Research Center "Kurchatov Institute" in Moscow and after three postdoctoral  
1520 stays at the MPI for Dynamics and Self-Organisation in Goettingen (2004-07), TU Berlin  
1521 (2007-09), and at Harvard (2009-11) he became a group leader at the MPI for the Physics  
1522 of Complex Systems in Dresden, Germany in 2011. In 2018 he became a chair (full  
1523 professor) of Mathematics in Life Sciences at the Friedrich-Alexander-University  
1524 Erlangen-Nuernberg. He is also a scientific board member of the recently founded Max-  
1525 Planck-Zentrum für Physik und Medizin in Erlangen. His group develops theoretical  
1526 models to understand complex biological phenomena and their implications in disease.  
1527 The group brings expertise in theoretical biophysics, statistical physics and numerical  
1528 methods and works in close collaboration with experimental groups.

1529  
1530 **Liraz Chai** is an Associate Professor of Chemistry at the Hebrew University of Jerusalem.  
1531 She holds a Ph.D. degree in Chemistry from the Weizmann Institute of Science (WIS,  
1532 2007), where she studied the intermolecular interactions between polymers- and charge-  
1533 bearing surfaces. Following a one year postdoctoral research at the WIS (2008), she  
1534 switched gears to microbiology in a second postdoctoral study at Harvard University  
1535 (2009-2013), where she studied bacterial biofilms. Liraz joined the Hebrew university as  
1536 Assistant Professor in 2014, and was promoted to Associate Prof. in 2022. Her research  
1537 combines Biochemistry, Soft Matter, Biophysics and Microbiology - all applied to an  
1538 interdisciplinary research of bacterial biofilms. Her major interest in biofilms include the  
1539 properties and assembly of extracellular matrix biopolymers, as well extracellular matrix  
1540 - associated biomineralization processes.

1541 **Klaus Dreisewerd** is a Professor of Biophysics at the University of Münster, Germany.  
1542 He graduated under the supervision of the MALDI pioneers Profs. Franz Hillenkamp and  
1543 Michael Karas, before moving to the Free University of Amsterdam in 1994 to co-establish  
1544 the MALDI technique for one of the early single-cell mass spectrometry studies as a  
1545 postdoc, then with a focus on brain neurons. Since his return to Münster University in  
1546 1997, he continues to work on methodological and instrumental advancements of the  
1547 MALDI technique, with a particular interest in the physical and physicochemical  
1548 fundamentals of the laser-based method. A strong application-driven research focus of  
1549 his group is on the advancement of highly-resolved MALDI imaging of biological tissues  
1550 including eukaryotic and microbial systems and its coupling with correlative microscopy.  
1551 The team collaborates closely with numerous partners, both from academia and industry  
1552 and recently introduced MALDI-2 and transmission-mode t-MALDI-2 mass spec imaging.

1553

1554 **Alexander Grünberger** is professor of “Microsystems in Bioprocess engineering at the  
1555 Karlsruhe Institute of Technology (KIT), Germany. He received his Dipl.-Ing. (2010) from  
1556 KIT and his Ph.D. (2015) from RWTH Aachen University in Germany. He underwent his  
1557 postdoctoral training under the supervision of Prof. Wolfgang Wiechert at the Research  
1558 Center Jülich in Germany. After being Junior Professor (W1) and Associate Professor  
1559 (W2) in biotechnology and bioprocess engineering at Bielefeld University, he became Full  
1560 Professor (W3) in “Microsystems for Bioprocess engineering” at KIT. His laboratory  
1561 focuses on the development and application of novel microfluidic tools for biotechnology  
1562 and bioprocess engineering. Current research activities focus on the development and  
1563 application of microfluidic single-cell cultivation tools and the understanding of microbial  
1564 phenotypic heterogeneity in the context of bioprocesses.

1565 **Christian Westendorf** is a research scientist at the Peter Debye Institute for Soft Matter  
1566 Physics at Leipzig University. He studied biology at the University of Rostock and  
1567 graduated in physics in 2012 at the Max Planck Institute for Dynamics and Self-  
1568 Organization (MPIDS) and Göttingen University, respectively. From 2013 to 2021 he  
1569 worked on biophysics of slime molds and complex flow patterns in the mammalian brain  
1570 during research stays at Graz University and MPIDS Göttingen. In 2021 he joined the lab  
1571 of Oskar Hallatschek at UC Berkeley and from 2022 onwards he works at Leipzig  
1572 University on the biophysics of bacterial evolution.

1573  
1574 **Susann Müller** received her diploma and PhD in biochemistry from the Martin Luther  
1575 University Halle-Wittenberg, Germany. In 2003 she habilitated in microbiology at the  
1576 Technical University of Dresden, Germany, and in 2011 she received an apl.  
1577 Professorship at the University of Leipzig. She was president of the German Society for  
1578 Flow Cytometry from 2008 to 2010. Her research at the Helmholtz Centre for  
1579 Environmental Research - UFZ Leipzig focuses on the ecology of microbial communities  
1580 in natural and managed systems using high-throughput technologies for single cell  
1581 analysis including cell sorting. Her current work is dedicated to elucidating ecological  
1582 mechanisms that control microbial communities, with a focus on situations that stabilize  
1583 communities in structure and function.

1584  
1585 **Thorsten Mascher** is a Professor of General Microbiology at the Technische Universität  
1586 Dresden, Germany. He received his PhD from the Universität Kaiserslautern (Germany)  
1587 in 2001. After a postdoctoral stay at Cornell University (2002-2003), he returned to  
1588 Germany as a research associate to start his own junior research group at the Georg-  
1589 August Universität Göttingen. In 2008, he accepted the position of an independent  
1590 research group leader at the Karlsruhe Institute of Technology. A year later, he was  
1591 appointed as Professor of Synthetic Biology at the Ludwig-Maximilians-Universität  
1592 München. Since 2022, he is Dean of the Faculty of Biology at the Technische Universität  
1593 Dresden and coordinator of the DFG-funded priority program SPP2389 “Emergent  
1594 Functions of Bacterial Multicellularity”. Current research topics include the role of  
1595 cannibalism toxins in multicellular differentiation of *Bacillus subtilis*, the regulation of their  
1596 biosynthesis, and functionalizing the endospore of *B. subtilis* for SynBio applications,  
1597 particularly in the context of engineered living materials.